Toxicology Reports 1 (2014) 923–944

Contents lists available at ScienceDirect

Toxicology Reports

journal homepage: www.elsevier.com/locate/toxrep

Bioactivity of nanosilver in *Caenorhabditis elegans*: Effects of size, coat, and shape

Piper Reid Hunt[a,*], Zachary Keltner[a], Xiugong Gao[a], Steven J. Oldenburg[b], Priyanka Bushana[a], Nicholas Olejnik[a], Robert L. Sprando[a]

[a] *Center for Food Safety and Applied Nutrition, FDA, Laurel, MD, United States*
[b] *nanoComposix Inc., San Diego, CA, United States*

ARTICLE INFO

Article history:
Received 12 August 2014
Received in revised form 23 October 2014
Accepted 24 October 2014
Available online 5 November 2014

Keywords:
Nanosilver
Ionic silver
Growth assay
Silver uptake
Physico-chemical properties
Alternative toxicity model

ABSTRACT

The in vivo toxicity to eukaryotes of nanosilver (AgNP) spheres and plates in two sizes each was assessed using the simple model organism *Caenorhabditis elegans*. For each shape, smaller AgNP size correlated with higher toxicity, as indicated by reduced larval growth. Smaller size also correlated with significant increases in silver uptake for silver nanospheres. Citrate coated silver spheres of 20 nm diameter induced an innate immune response that increased or held steady over 24 h, while regulation of genes involved in metal metabolism peaked at 4 h and subsequently decreased. For AgNP spheres, coating altered bioactivity, with a toxicity ranking of polyethylene glycol (PEG) > polyvinylpyrrolidone (PVP) ≅ branched polyethyleneimine (BPEI) > citrate, but silver uptake ranking of PEG > PVP > citrate > BPEI. Our findings in *C. elegans* correlate well with findings in rodents for AgNP size vs. uptake and toxicity, as well as for induction of immune effectors, while using methods that are faster and far less expensive, supporting the use of *C. elegans* as an alternative model for early toxicity screening.

1. Introduction

Nanoparticles (NP) are defined as objects that measure between 1 and 100 nm in at least one dimension. Given that the diameter of many cellular macromolecules such as DNA (2 nm) [1], ATP synthase (10 nm) [2], and synaptic vesicles (40 nm) [3] are also in this size range, it is perhaps unsurprising that NP can exhibit bioactivities that are lacking in corresponding bulk materials. NP can be synthesized using a variety of base materials in different sizes and shapes, with each parameter conferring specific physical and bioactive properties [4]. As a result, investigations of novel uses for NP with applications in fields such as electronics, medicine, and food packaging are increasing rapidly [5]. Due to the recent growth in the availability of consumer products that contain NP [6], it has been estimated that gross sales could top one trillion dollars per year by 2015 [7].

Nanosilver (AgNP) has both antibacterial and antiviral activity [8–10], and in in vitro studies has been shown to be as effective as standard antibiotics against several clinically relevant strains of pathogenic bacteria [11,12]. The antimicrobial properties of AgNP have led to a dramatic increase in the availability of commercial products and medical devices that contain AgNP, with estimates of the amount AgNP manufactured per year exceeding 300 tons [13]. While there has also been growth in the number of studies conducted investigating the safety of NP exposure, many lack adequate nanomaterial characterization and/or do not report dosing methods [14]. Additionally, ionic silver

* Corresponding author. Tel.: +1 240 402-3420.
E-mail address: Piper.Hunt@fda.hhs.gov (P.R. Hunt).

http://dx.doi.org/10.1016/j.toxrep.2014.10.020

(Ag^+) can be released from the surface of AgNP in solution [15], yet only a small minority of studies report on the toxicity of supernatants or filtrates of AgNP solutions so that the toxicity of applied AgNP can be evaluated separately from the toxicity of impurities acquired during synthesis, or Ag^+ released during storage [16].

Qualities that can alter the stability and biological response to AgNPs include size, shape, coating, and manufacturing methods. For AgNP spheres, smaller size is associated with increased antibacterial activity [9,17], increased toxicity to zebrafish embryos [18], and higher cytotoxicity and inflammatory marker release in mammalian cell culture models [19]. Silver nanoplates (AgPlates) are high aspect ratio particles that can be used for photoacoustic imaging in medical diagnostics [20]. AgPlates have higher antibacterial activity against *Escherichia coli* than silver nanospheres or rods [21]. Additionally, silver nanoplates were found to be more toxic to zebrafish than silver nanospheres or wires, though this effect was attributed to crystal defects on the surface of the plates having a negative impact when in contact with cellular membranes [22], indicating that different synthesis methods may improve eukaryotic tolerance.

Coats or capping agents are used to stabilize NP in solution by altering surface charge or introducing steric repulsion. One of the most commonly used AgNP stabilizing agents is citrate, which gives the resultant particles a negative surface charge [23,24]. Polyvinylpyrrolidone (PVP) is a polar, hygroscopic compound used as a wetting or binding agent for cosmetics and pharmaceuticals. PVP also imparts a slight negative charge to AgNP, though less than citrate [15]. In zebrafish embryos, PVP coated AgNP is more toxic than citrate coated AgNP of the same size and shape [18]. Branched polyethyleneimine (BPEI) is a relatively new coating material for NP which provides a positive surface charge due to amino and amide groups [25]. Positively charged amine groups have been shown to increase NP protein absorption and cell membrane interactions in vitro [26], but information on how positively charged NPs behave in vivo is scarce. Polyethylene glycol (PEG) is manufactured in a variety of molecular weights and chemical variants for use in processed foods and pharmaceuticals. PEGylation of NP inhibits agglomeration and protein absorption [27]. While it is known that functional coatings can alter the bioactivity of NP [28], there are only a few published studies on the relative toxicity of different coats on NPs of a specific size and shape. Base material and synthesis methods can also alter NP toxicological profiles [29,30], making generalized safety assessments difficult. Therefore, it is important that each NP species be tested individually, in a model that is appropriate for assessed exposure route [31].

In vitro toxicity testing using cellular models is simple, fast, and inexpensive when compared to traditional in vivo toxicity testing using mammals, yet results from in vitro tests using cellular models frequently do not correlate with in vivo data [32]. Another drawback of many types of in vitro models for predictive toxicology is that they cannot mimic the effects of biological fluids or enzymatic metabolism that occurs in vivo [33]. Therefore, a small whole animal model such as the microscopic soil dwelling nematode *Caenorhabditis elegans* is likely to prove more predictive for oral toxicity screening than cell based assays. *C. elegans* have a short generation time and are easily maintained under laboratory conditions in axenic media. Many types of assays in *C. elegans* can be completed in a week or less. Previously, we and others have demonstrated that *C. elegans* assays can predict mammalian toxicity ranking [34–36], and that 10 nm AgNP spheres, while toxic to *C. elegans* at high concentration, are less toxic than Ag^+, which also correlates with data from in vivo rodent and in vitro mammalian cell culture studies [30]. Here we assess the effects of AgNP size, shape, and coat on bioactivity in *C. elegans* using larval growth assays, organismal silver uptake measurements, and gene expression.

2. Materials and methods

2.1. Reagents and test materials

ReagentPlus grade silver acetate was purchased from Sigma–Aldrich, and fresh solutions of 1 mg/mL silver ion (Ag^+) equaling 1.55 mg/mL silver acetate were prepared weekly. For evaluations of NP coat toxicity, mPEG-OH, MW 5000 was supplied by Laysan Bio; citrate, PVP, and BPEI were supplied in solution by nanoComposix. BioPure NPs were purchased from nanoComposix (San Diego, CA). The manufacturer characterizes each batch with transmission electron microscopy (TEM) to determine size and shape distributions, UV-visible spectroscopy to measure the optical properties, particle hydrodynamic diameter with dynamic light scattering, and particle surface charge with a zeta potential measurement. BioPure NPs are extensively washed with the suspending solvent to remove residual reactants from the manufacturing process. Mass concentration is determined with inductively coupled plasma mass spectroscopy (ICP-MS). The particles are sterile filtered and tested for endotoxin contamination before delivery. Throughout the study, nanomaterials were stored at 4 °C and tested regularly by dilution in diH_2O followed by UV-visible spectroscopy (UV-vis) using a UV-1800 (Shimadzu) to verify the stability of each NP suspension. NPs with altered UV–vis spectra were replaced. For assessment of agglomeration or degradation effects in nutrient media, NPs were also mixed to 100 μg/mL in CeHM as above, then diluted 1:20 in diH_2O, and tested by UV–vis. Supernatants of all test articles were obtained by high-speed centrifugation of silver suspensions according to published guidelines [37]. Briefly, suspensions of 10nmAgCit were subjected to centrifugation at 40,000 × *g* for 120 min, and all other AgNP suspensions at 25,000 × *g* for 90 min, with a WX Ultra Series centrifuge in a F50L-24 × 1.5 rotor (ThermoScientific). Supernatants were carefully separated from pellets and assessed for toxicity and silver concentration.

2.2. Experimental design

C. elegans feed by pharyngeal pumping, which pulls liquid phase components from their surroundings into their digestive system, making them a good model for oral toxicity as test articles can be applied to the media in which they are maintained. Some of the endpoints and methods

Table 1
Some screening options for the *C. elegans* oral toxicity model.

Test category	Assay	*C. elegans*	Method(s)	Exposure duration	Details
Toxicity assessments	Adult Death	Synchronized adults	Manual manipulation + visual assessment of movement response Fluorescent detection of dyes that accumulate in dead cells	Test article (TA) dependent, high concentrations required for a 24 h test are limited by solubility	Oral toxicity model in adults correlates with mammal LD_{50} assessment methods
	Larval growth	Synchronized first larval stage (L1s)	Visual assessment of maturity Body length measurements via microfluidics + laser detection	Often 3–7 days, depending on TA response Time for control L1s to mature into adults, ~3 days depending on conditions	Larval growth assays are a more sensitive measure of toxicity than adult LD_{50} for toxin ranking
	Motility	Dependent on size detection limits of tracking method	Video microscopy + tracking software Beam interruption detection	Dependent on TA response and test medium (swimming in liquid vs. crawling on agar)	Some TAs can alter motility at concentrations far lower than those detected by other endpoints
Toxin response	Gene expression	Synchronized adults	Microarrays and/or RT-PCR	Gene expression response can peak within a few hours of exposure, and frequently normalizes with exposures >1 day	Toxins can suppress larval development, use of adults avoids confusion of toxin response with larval stage specific gene expression
		Variable	Transgenic strains with fluorescent-tagged genes	Hours to days, dependent on sufficient accumulation of expressed transgene	Limited by transgenic strain development
Test article uptake	Average organismal [TA]	Synchronized adults	ICP-MS (elemental analysis)	Dependent on TA concentration and limits of detection method	Use of adults and low [TA] reduces chance of decreased uptake due to toxic response

that can be used to screen for toxicity in *C. elegans* are outlined in Table 1. Generally, very high concentrations of test articles are needed to identify LD_{50} concentrations in *C. elegans* adults, which can lead to solubility issues [36]. Delayed development is a far more sensitive measure of toxin response, therefore larval growth assays were selected to assess the toxicity of AgNP species in relation to each other for ranking. However, since toxins can alter the timing of *C. elegans* development, the use of larvae for genetic response to toxin exposure is problematic, as many genes have larval stage specific expression patterns. For this reason, *C. elegans* adults were used to assess gene expression. In order to ensure a response while avoiding non-specific gene expression changes secondary to tissue damage or necrosis, morphology and motility assessments were utilized to select test article concentrations with similarly low levels of toxicity for microarray experiments. In contrast to gene expression, comparisons of uptake require that the dose of silver be the same for all silver species, therefore a single lower silver concentration was selected for uptake assessments in order to avoid damage to intestinal epithelia, which can alter test article uptake.

2.3. Culture and dosing of C. elegans

The *C. elegans* wild type N2 Bristol strain used in these experiments was provided by the *Caenorhabditis* Genetics Center, which is funded by the NIH National Center for Research Resources. *C. elegans* were maintained at 20 °C in *C. elegans* Habitation Media (CeHM), an axenic media composed of *C. elegans* Habitation Reagent (CeHR), water, and organic non-fat cows' milk [34]. Dosing solutions were prepared fresh for each experiment by first diluting AgNPs into diH_2O with sonication at twice the highest final dosing concentration, followed by further dilution when required, and then mixed in the order: 5 parts diH_2O or diluted test article to 2 parts milk to 3 parts CeHR. For dosing of adults, synchronized *C. elegans* were first treated with 5-Fluoro-2′-deoxyuridine (FUdR) to prevent progeny production at 56 h post-first larval stage (L1) feeding [36], and then dosed the following morning.

2.4. Larval growth assessment

Automated assessment of time-of-flight (TOF) with the COPAS™ Biosort (Union Biometrica) was used to assess the length of a minimum of 500 *C. elegans* per treatment, grown for 3 days at 20 °C from L1 in dosed CeHM. Data presented is the mean standardized TOF indicated *C. elegans* body length ±SD from a minimum of 3 separate trials. Small changes in temperature and nutrient concentration are associated with altered *C. elegans* larval growth rate. When working with small volumes required for even medium throughput screening, it is impractical to control temperature such that all wells are within 0.5° C of each other at all times. Even without mistakes such as handling plates in such a way as to temporarily warm the contents, changes in barometric pressure and ambient temperature can influence COPAS flow rate, altering readout. For these reasons, within a single well-executed experiment, TOF can vary

among controls by more than 10%. Therefore, we have not considered mean TOF reductions of 15% or less from the control to be biologically significant for the purposes of this screen.

2.5. C. elegans motility assessment

Automated assessment of average locomotive activity within each treatment group was done using a WMicrotracker-One™ (PhylumTech), which records movement as photo-beam interruptions (bins) within wells of 12-well plates. Motility assessments were conducted in an incubator at 20 °C with all reagents given 2 h to equilibrate to temperature. Briefly, approximately 1000 freshly fed synchronized adult *C. elegans* in 900 μL CeHM were placed in wells and allowed to adapt to the well for 1 h, followed by a 60 min baseline motility assessment in the WMicrotracker. 100 μL of water or 10× dosing solution were then added to each well, and plates were returned to the WMicrotracker. Data was sampled in 60-min blocks, divided by the baseline reading, and then normalized to the water control. Each experiment was done in duplicate and repeated on three separate days.

2.6. ICP-MS for silver concentration and uptake assessment

To assess tissue uptake of silver, approximately two thousand synchronized adult *C. elegans* were exposed to 25 μg/mL AgNP or Ag^+ for 24 h, washed in M9 buffer, returned to CeHM for half an hour to flush silver from the digestive tract, washed again, and then frozen for subsequent ICP-MS analysis. Worm pellets were digested in PFA vessels with 1 mL DI water and 2 mL concentrated nitric acid. A MARSXpress microwave digestion system (CEM Corporation) was used with a temperature program consisting of a 15 min ramp to 200 °C and a 15 min hold at 200 °C. After cooling, extracts were transferred to 50 mL vials and 125 μL concentrated HCl was added, followed by dilution to a final volume of 25 mL. Analysis was performed on an X Series II ICP-MS (Thermo Scientific) equipped with on-line internal standard delivery, PC3 Peltier Chiller and SC-2 DX autosampler (both from Elemental Scientific). Total silver was analyzed using m/z 107 and Ge and Sc as internal standards. Calibration standards were prepared by dilution from a 1000 ppm silver standard (Inorganic Ventures). Calibration curve was verified for each analysis using dilutions from a 1 ppm silver standard (Spex Certiprep). Recoveries were verified for each analysis using NIST 1556b standard reference material (NIST), and control worm aliquots spiked with silver standard.

2.7. Microarray analysis

Adult *C. elegans* were exposed to test articles in CeHM for indicated times, washed in M9 buffer, suspended in QIAzol Lysis Reagent (QIAGEN) and then frozen at −80 °C. Total RNA was isolated using the EZ1 RNA Universal Tissue Kit (Qiagen) with the EZ1 Advanced XL (Qiagen) automated RNA purification instrument following the manufacturer's protocol, including an on-column DNase digestion. RNA concentration and purity were measured with the NanoDrop 2000 UV-Vis spectrophotometer (NanoDrop Products). Integrity of RNA samples was assessed with the RNA 6000 Nano Reagent Kit using the Agilent 2100 Bioanalyzer (both from Agilent). Total RNA samples were preprocessed using the Affymetrix GeneChip 3′ IVT Express Kit following the manufacturer's protocol for hybridization to GeneChip *C. elegans* Array (Affymetrix). Affymetrix GeneChip Hybridization, Wash, and Stain Kit was used following the manufacturer's protocol. The chips were scanned on Affymetrix GeneChip Scanner 3000 7G, and the image (.DAT) files were preprocessed using the Affymetrix GeneChip Command Console (AGCC) software v.4.0 to generate cell intensity (.CEL) files. Data quality was assessed using the Affymetrix Expression Console software v.1.3, and all quality assessment metrics (including spike-in controls during target preparation and hybridization) were found within boundaries. Microarray data analysis was carried out primarily using the U.S. FDA's ArrayTrack software system [38]. The values of individual probes belonging to one probe set in .CEL files were summarized using the robust multi-array average (RMA) algorithm [39] embedded in ArrayTrack, which performs convolution background correction, quantile normalization, and median polish summarization. Differentially expressed genes were selected using one-way analysis of variance (ANOVA) based on Welch t-test. To improve moderated t-statistics, the I/NI-calls gene filtering procedure [40] was applied before the Welch t-test to exclude non-informative genes. For each comparison between two experimental groups, the fold change (FC) of every annotated gene, together with their corresponding p-value, was used for selection of differentially expressed genes with cutoffs of $p < 0.05$ and FC > 1.5.

3. Results

3.1. Nanoparticle characterization

In order to correlate the effects of nanoparticle (NP) size, shape and coating to observed bioactivity, it is critical that the physicochemical state of the NP is measured and monitored. Transmission Electron Micrographs (TEM) images demonstrate the uniformity of the size and shape of the particles. The zeta potential of the particles, which provides information on the particle surface charge, is an important determinant of subsequent nanoparticle interactions. NP coating, zeta potential, average diameter as measured by TEM, and hydrodynamic diameter as measured by dynamic light scattering are shown in Table 2. Zeta potential values of the citrate and PVP coated particles are negative, BPEI coated particles are strongly positive, and the PEG coated silver nanoparticles have a more neutral charge. The optical properties of silver nanoparticle solutions also provide important information. At the nanoscale, silver particles have unique optical properties due to their plasmon resonance that are a function of the nanoparticle's size, shape, and aggregation state [41]. By monitoring the UV–visible (UV–vis) spectrum of the particles as received, and after dilution in axenic *C. elegans* Habitation Media (CeHM), the aggregation state of the nanoparticles can be tracked

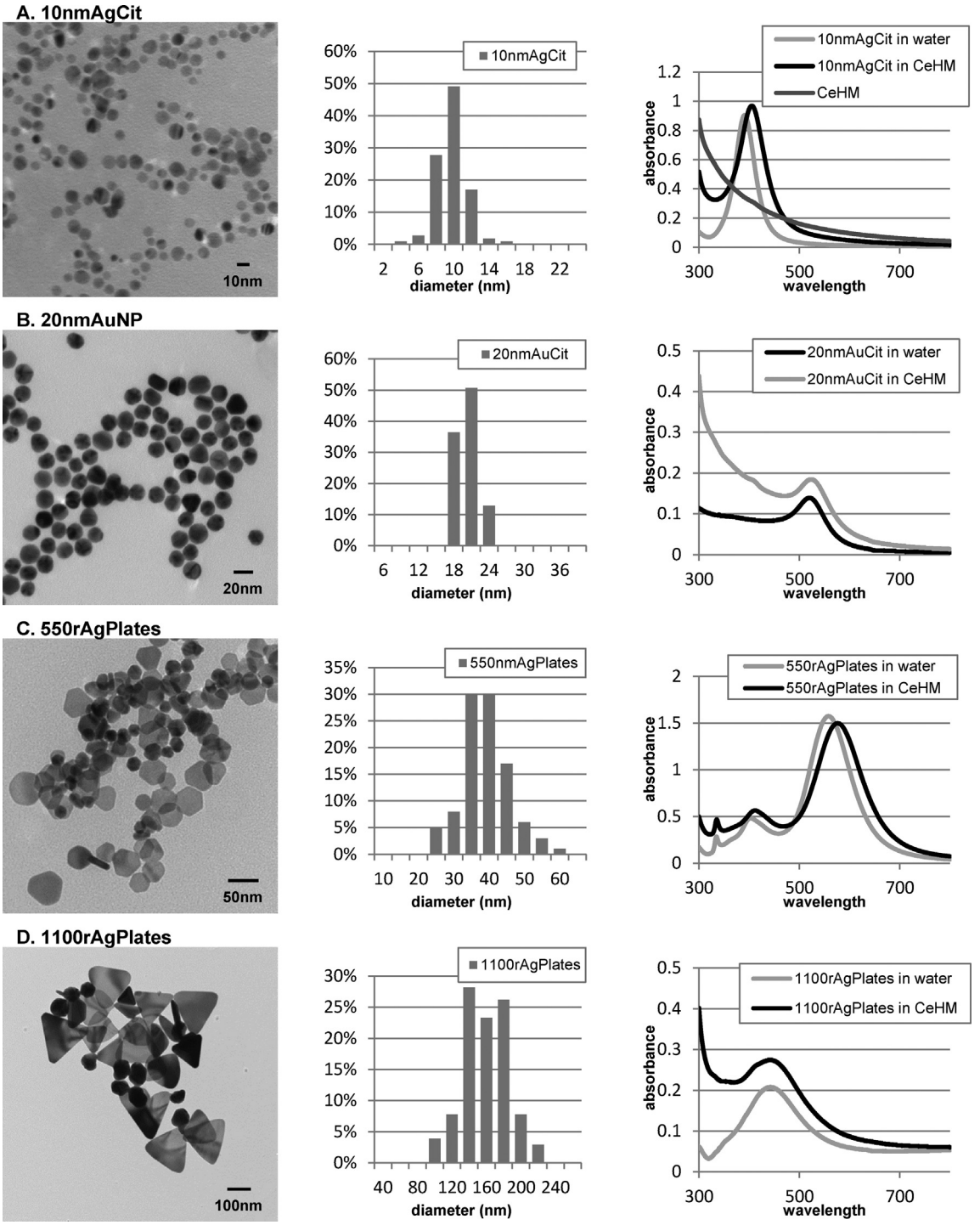

Fig. 1. Nanomaterial characterization figure shows representative transmission electron microscopy images (column 1), size histograms for a minimum of 75 particles counted (column 2), and UV-visible spectroscopy for nanoparticles dispersed in water (light gray) or CeHM (*C. elegans* Habitation Media, black), and CeHM alone (dark gray) (column 3). (A) Citrated coated ~10 nm diameter silver nanospheres (10nmAgCit). (B) Citrate coated ~20 nm diameter gold nanospheres (20nmAuNP). (C) PVP coated silver nanoplates with resonance at 550 nm (550rAgPlates). (D) PVP coated silver nanoplates with resonance at 1100 nm (1100rAgPlates). (E) Citrated coated ~20 nm diameter silver nanospheres (20nmAgCit). (F) BPEI coated ~20 nm diameter silver nanospheres (20nmAgBPEI). (G) PVP coated ~20 nm diameter silver nanospheres (20nmAgPVP). (H) PEG coated ~20 nm diameter silver nanospheres (20nmAgPEG). (I) Citrated coated ~110 nm diameter silver nanospheres (110nmAgCit). (J) PVP coated ~110 nm diameter silver nanospheres (110nmAgPVP). (K) PEG coated ~110 nm diameter silver nanospheres (110nmAgPEG).

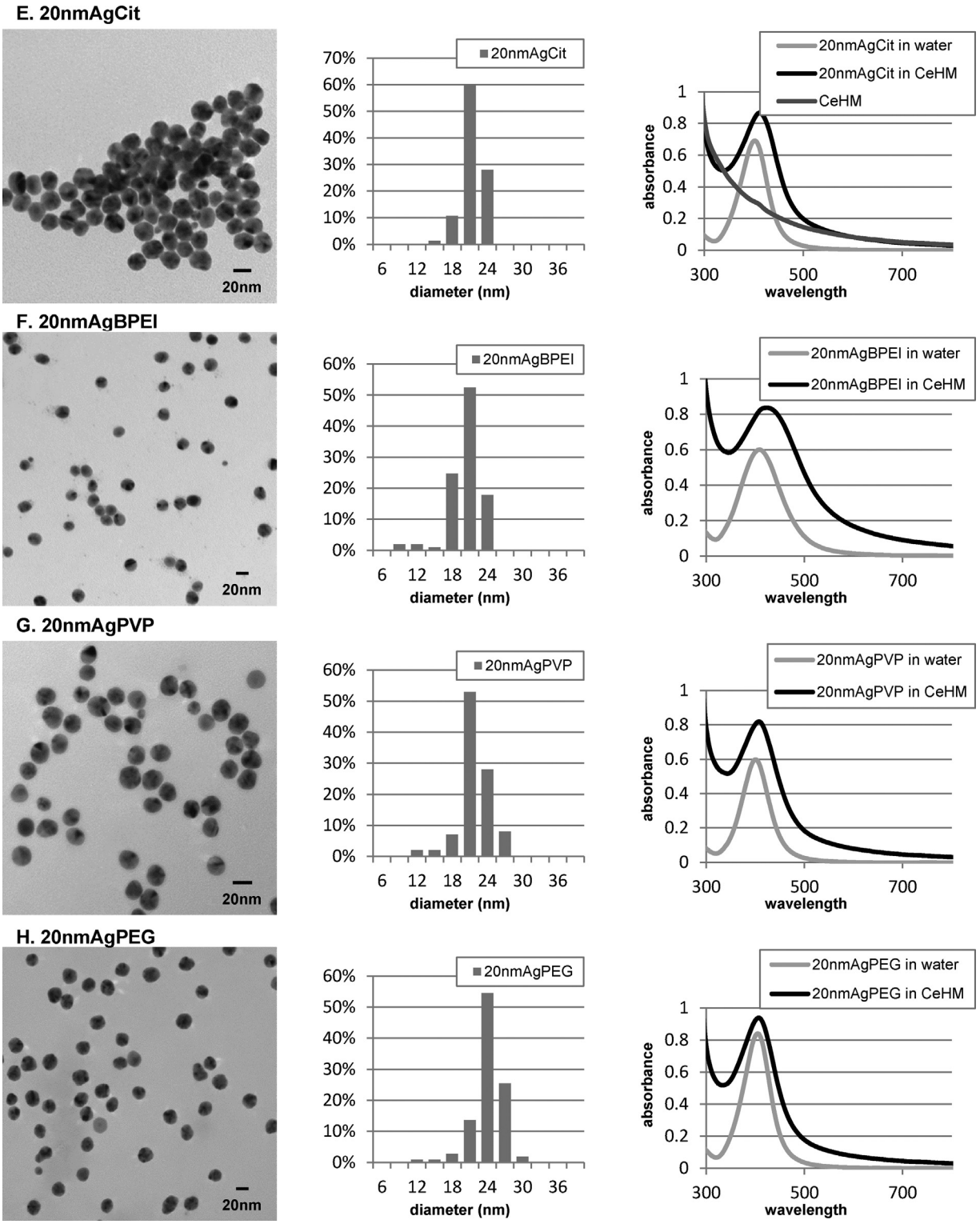

Fig. 1. (*Continued*)

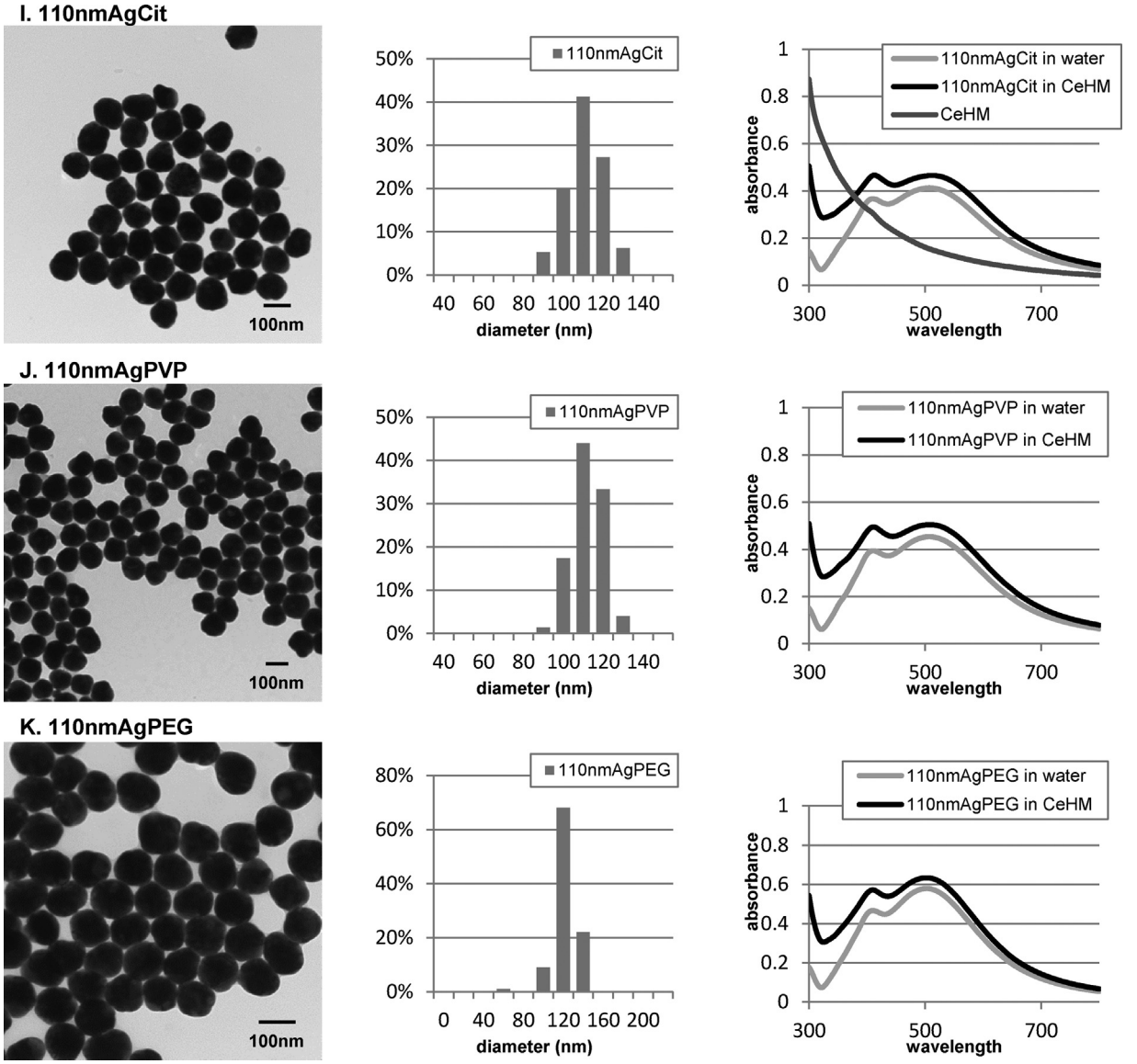

Fig. 1. (*Continued.*)

optically. Any aggregation of the nanoparticles will reduce the intensity and broaden the peaks in the silver nanoparticle spectrum. Fig. 1 shows representative TEM images, size histograms and the UV–vis spectra for the NP utilized in this study. The difference between the nanoparticle spectra before and after suspension in *C. elegans* Habitation Medium (CeHM) is primarily due to the background absorbance of the CeHM media itself, indicating that the silver nanoparticles remained stable and unagglomerated after combination.

3.2. Effect of size on nanosilver toxicity

The effects of size on the toxicity of nanosilver (AgNP) were assessed using larval growth assays. Synchronized first larval stage (L1) *C. elegans* were exposed for 3 days to suspensions or supernatants of citrate coated AgNP spheres of 10, 20, and 110 nm diameter (10nmAgCit, 20nmAgCit, and 110nmAgCit, respectively) at concentrations ranging from 6.25 μg/mL to 100 μg/mL. Equivalent masses of ionic silver (Ag^+) in the form of silver acetate, and starved L1s maintained in non-nutrient M9 buffer were used as positive controls. At 100 μg/mL silver, relative to controls, length was at $93 \pm 7\%$ ($p > 0.1$, $n = 4$ trials) for 110nmAgCit, $74 \pm 5\%$ ($p < 0.001$, $n = 6$) for 20nmAgCit, $41 \pm 6\%$ ($p < 0.001$, $n = 4$) for 10nmAgCit, and $26 \pm 3\%$ ($p < 0.001$, $n = 5$) for Ag^+. Thus, 10nmAgCit reduced larval growth more than 20nmAgCit, 110nmAgCit did not significantly reduce larval growth at tested concentrations, and Ag^+ reduced larval growth more than any AgNP tested (Fig. 2A), indicating that AgNPs are less toxic than Ag^+, and for citrate coated AgNP spheres, decreasing size correlates with increasing toxicity.

Table 2
Nanomaterial characterization.

NP abbreviation	Base material	Coat[a]	Zeta potential (mV)	Average diameter (nm)	Count	Std. Dev.	Min/Max diameter (nm)	Hydro-dynamic diameter (nm)
20nmAgCit	Silver	Citrate	−37	19.8	75	2.0	12.4/23.6	25.5
20nmAgBPEI	Silver	BPEI	53	18.7	101	2.6	8.3/23.0	54.8
20nmAgPVP	Silver	PVP	−28	20.4	100	2.7	10.0/25.6	24.3
20nmAgPEG	Silver	PEG	−17	22.9	110	2.8	9.4/28.6	44.3
110nmAgCit	Silver	Citrate	−44	106.2	114	9.2	82.5/126.1	115.1
110nmAgPVP	Silver	PVP	−29	107.9	75	7.2	88.2/123.5	128.6
110nmAgPEG	Silver	PEG	0.4	111.4	100	10.7	47.2/136.8	127.4
10nmAgCit	Silver	Citrate	−36	8.8	112	1.7	3.9/15.9	14.1
20nmAuNP	Gold	Citrate	−40	18.7	140	1.7	15.7/23.4	21.7
550rAgPlates	Silver	PVP	–	36.6	100	6.6	20.1/56.9	N/A (plates absorbance too close to laser)
1100rAgPlates	Silver	PVP	−16	149.1	103	27.5	80.3/210.9	164

Characterization data from nanomaterials used in this study.
[a] Particles were surface functionalized with citrate, branched polyethyleneimine (BPEI), polyvinylpyrrolidone (PVP), or polyethylene glycol (PEG).

All NP used in this study were nanoComposix BioPure grade nanoparticles, which are washed with >5 volumes of the buffer to ensure that all manufacturing byproducts are removed, as these reaction byproducts can be responsible for toxicity mistakenly attributed to the nanomaterial itself [23,24]. Additionally, Ag^+ can be released from the surface of AgNP over time, altering the toxicity profile of AgNP suspensions [15,42]. We therefore also assessed citrate buffer alone as well as AgNP soluble fractions for toxicity. No reduction in larval growth was observed after exposure to citrate buffer at experiment relevant concentrations (Supp. Fig. 1A) or to high-speed supernatants of 10nmAgCit, 20nmAgCit, or 110nmAgCit (Supp. Fig. 1B), while both suspensions and high-speed supernatants of Ag^+ suppressed larval growth to similar extents (Fig. 2A). This indicates that the toxicity associated with 10nmAgCit and 20nmAgCit was due to NP exposure and not soluble impurities or Ag^+ released from the surface of AgNP during synthesis or storage. It also demonstrates that soluble Ag^+ is not removed from suspension by high-speed centrifugation.

To assess the effects of AgNP size on silver uptake, we tested *C. elegans* adults exposed to 25 μg/mL AgNP or Ag^+ for one day by ICP-MS for total organismal silver concentration. For 110nmAgCit, 20nmAgCit, 10nmAgCit, and Ag^+, decreasing size correlated with increasing silver uptake (Fig. 2B). The observed variability of silver uptake with Ag^+ (Fig. 2B) is likely do to a threshold toxicity effect altering intestinal function in some experiments. In summary, for citrated coated AgNP spheres, increasing silver uptake correlated with increasing toxicity. Worms exposed to high-speed AgNP supernatants grew at a normal rate and had barely detectable levels of silver. ICP-MS assessment of AgNP suspensions confirmed similar silver concentrations in each, with very low levels of silver in the corresponding AgNP high-speed supernatants (Fig. 2C). In contrast, equivalent concentrations of silver were found in Ag^+ suspensions and high-speed supernatants, indicating that if Ag^+ had been released from AgNP surfaces, it would have been detected in the AgNP high-speed supernatants.

3.3. Microarray assessment of gene regulation

To shed light on the mechanisms of AgNP effects, we selected 20nmAgCit as a representative AgNP species for microarray analysis. *C. elegans* adults were exposed to 100 μg/mL 20nmAgCit in CeHM for 4, 8 or 24 h. Innate immune response *Caenorhabditis* bacteriocin (CNC) genes *cnc-2*, *cnc-4*, *cnc-6*, and *cnc-7* all showed greater up regulation at 24 h than at earlier time points (Table 3). The *nlp-31* gene has been shown to be up regulated in *C. elegans* in response to fungal infection, and synthetic NLP-31 has antimicrobial activity in vitro [43]. Exposure to 20nmAgCit for 8 or 24 h induced up regulation of *nlp-31*, but 4 h exposure did not, consistent with a late innate immune response. Similarly, fungus induced proteins *fip-1*, *fip-5*, and *fipr-26* were all up regulated by 20nmAgCit at 24 h but not at 4 or 8 h. Other highly regulated late response genes included *ZK970.7* (a gene that is up regulated by bacterial infection [44], up 10.0-fold at 24 h), *far-4* (encodes a fatty acid/retinol binding protein, up 7-fold at 24 h), and two genes with unknown function, *F07B7.8* (up 6.1-fold at 24 h) and *H39E23.3* (up 5.1-fold at 24 h).

In contrast to the immune response, several canonical metal response genes showed early peaks followed by decreasing regulation over the 24 h assessment period. For example, *hmt-1* (Heavy Metal Tolerance Factor) was up regulated by 20nmAgNP exposure 2.3-fold at 4 h but only 1.5-fold at 24 h, *ftn-1* (a *C. elegans* gene with high homology to human ferritin heavy chain FTH1 [44]), was up regulated 1.7-fold at the 4 h time point only, and *numr-1* (NUclear localized Metal Responsive) was up regulated 17-fold at 4 h, 5.1-fold at 8 h, but less than 2-fold at 24 h. Many glutathione S-transferases (GST) and UDP-glucuronosyltransferases (UGT) are involved in phase II xenobiotic detoxification processes [45,46]. All six GST genes (*gst-5*, *gst-9*, *gst-12*, *gst-14*, *gst-30* and *gst-31*) and all three UGT genes (*ugt-3*, *ugt-9*, and *ugt-20*) differentially regulated by 20nmAgCit also showed this pattern of early up regulation (Table 3 and Supplemental Excel Data).

Over the three assessed time points, the expression of a total of 141 genes was significantly altered with

Table 3
Genes differentially regulated by exposure to 20nmAgCit or Ag^+.

Gene		Category	Fold Δ 20nmAgNP					Fold Δ Ag^+	
Name	Sequence		#1 4 h	#2 4 h	#1 8 h	#1 24 h	#2 24 h	#2 4 h	#2 24 h
Early or decreasing response to 20nmAgCit									
clec-7	F10G2.3	–	0.5	0.4	0.6				0.6
comt-3	Y40B10A.2	Imm [2], Metal [33,35], Xen/Str [5,14]	2.2	1.9				4.8	1.6
comt-4	40B10A.6	Imm [29], Metal [60], Xen/Str [5]	6.9	5.5	2.4	1.8	1.6	23	2.9
cpr-3	T10H4.12	Imm [2,29,65,84], Endo/Lyso [3]		2.2	1.6			4.3	1.8
fipr-22	C37A5.2	Imm [28]						14	2.4
fipr-23	C37A5.4	Imm [28]						11	2.1
folt-2	F37B4.7	Imm [29], Metal [35], DR [27]						0.2	
ftn-1	C54F6.14	↑ Imm [28], Metal [33], Xen/Str [9,24], DR [27]	1.7	2.4				13	0.5
gst-12	F37B1.2	Metal [33,35], Xen/Str [14,46,76]	3.9	2.7	2.2	1.6		2.1	
gst-30	ZK546.11	Metal [33,35], Xen/Str [14,76]	2.4	2.3	2.0			4.3	
gst-31	Y53F4B.35	Metal [33,35]	2.7	2.5	1.6				
gst-9	R05F9.5	Metal [33,35], Xen/Str [14,76]	3.7	2.4	1.9				
hmt-1	W09D6.6	Metal [9], Mitoc [9]	2.3	2.3	1.7	1.5		5.8	1.8
hsp-16.1	T27E4.8	↑ Metal [35,45], Xen/Str [14,22]		0.6				5.8	
ins-7	ZK1251.2	Imm [84,86]			1.7			5.1	
lact-1	F46H5.8	Imm [42]	2.7	1.7				5.0	
msd-1	F44D12.3	–		0.5					
nlp-26	Y43F8C.2	–	6.9	4.0	3.4	1.6		5.9	
numr-1	F08F8.5	Metal [33,35,60], Xen/Str [14]	17	27	5.1	1.8	1.7	81	2.4
oac-6	C31A11.5	Imm [29,65], Metal [35,60], Xen/Str [14]		1.8				6.5	
pho-13	F07H5.9	Imm [29]		0.4				0.2	
pmp-5	T10H9.5	Imm [29], Metal [60], Perox [9]		0.6				0.2	
sams-1	C49F5.1	Imm [29], DR [9]						0.2	
scl-2	F49E11.10	↑Imm [65], ↓ Imm [42]						5.3	0.4
tsp-1	C02F5.8	Imm [29,65,84,85]		2.0				5.8	1.6
tsp-10	T14B4.4	–						0.2	
tsp-2	C02F5.11	Imm [29,65]		1.9				5.2	1.8
ttr-23	T21C9.8	Imm [29]		1.9	1.7			9.8	2.2
ugt-18	ZC443.5	Imm [29,65]		2.3				8.3	
ugt-3	ZC455.3	Metal [35]	6.7	4.1				84	
ugt-63	C04F5.7	–						0.1	
ugt-9	T19H12.1	Metal [35], Xen/Str [71,87]	2.0	1.9					
	B0024.4	Imm[29,40,65], Metal [60], Xen/Str [87]		2.6	2.4			2.4	11
	C05D9.9	Imm [29]						5.0	
	C17H12.6	Imm [2,29], Metal [33,35]	1.6	2.4	1.6			2.0	
	C28C12.4	Metal [35]	4.5	4.3	3.0	2.5	1.9	19	5.0
	C42D4.3	Xen/Str [20]						8.6	
	C45B2.2	Xen/Str [14]	3.6	2.9	2.0			5.0	1.8
	C45B2.3	Metal [35]	2.1	5.2	1.6			41	
	C50F7.5	Imm [29]						20	
	D1086.3	Imm [29], Metal [35]	0.6	0.4	0.6			0.3	
	F01D4.8	Xen/Str [20]						7.4	
	F23F12.12	–	0.5						
	F46F2.3	Imm [29]						0.2	
	F47B8.2	Imm [65], Metal [35]	2.5	2.4	1.8	1.6		5.0	1.7
	F49H6.13	Imm [29]		2.2					
	F53A9.2	Imm [29], Xen/Str [14]		2.3				2.9	
	F57H12.6	Xen/Str [22]	27	21	17	5.3	3.3	57	7.3
	K01C8.1	Metal [35]		0.5					
	R07E5.4	Imm [29], Endo/Lyso [9]		0.5				0.4	
	T05E12.6	Imm [29]						0.2	

Table 3 (*Continued*)

Gene		Category	Fold Δ 20nmAgNP					Fold Δ Ag^+	
Name	Sequence		#1 4 h	#2 4 h	#1 8 h	#1 24 h	#2 24 h	#2 4 h	#2 24 h
	T19D12.4	Imm [2,29], Metal [35]		2.2				2.0	
	T24C4.4	Imm [29]		3.2	1.6			4.2	
	T28H10.3	Imm [47,65], Endo/Lyso [3]						6.1	
	W03G1.5	Metal [35]	2.0	1.8				10	
	ZK105.5	–		0.5				0.6	
	ZK742.3	Metal [60], Xen/Str [14]	1.8					5.6	
	ZK742.4	Metal [33,35], Xen/Str [14,76], Lipid [9]	2.8	2.3	1.9	1.6	1.5	2.8	1.8
Late or increasing response to 20nmAgCit									
acdh-1	C55B7.4	Imm [2,29,47,84], Metal [35], Lipid [48] predicted to be a mitochondrial enzyme that catalyzes the first step of fatty acid beta-oxidation and thus plays a key role in energy production					0.5	0.2	
clec-17	E03H4.10	Imm [29,40,65], Xen/Str [30]			1.7	2.0	1.6	2.4	1.8
clec-60	ZK666.6	Imm [36,83], Metal [35], Xen/Str [87]					0.5		0.3
cnc-2	R09B5.3	Imm [29,39,41]	3.4	1.8	3.5	5.0	4.0	4.8	4.1
cnc-4	R09B5.9	Imm [28,29,41]	2.3	1.7	4.9	4.1	3.7	7.7	4.4
cnc-6	Y46E12A.1	Imm [29,41], Metal [35]	1.5		2.3	9.8	6.5	18	16
cnc-7	F53H2.2	Imm [28]	1.8	1.8	3.1	6.1	3.9	11	2.9
dhs-25	F09E10.3	Imm [29,65], Mitoc [9]					0.6		0.3
dod-21	C32H11.9	Metal [18,35]	1.6	2.3	1.9	2.9	7.3		15
far-4	F15B9.2	Metal [35], Lipid [9]	1.5		3.5	7.1	6.6		8.8
fip-1	F22B7.4	Imm [41]				3.5	3.4		13
fip-5	F41E7.4	Imm [9]				2.0	1.6	1.9	2.1
fipr-26	F53B6.8	Imm [42], Xen/Str [14]				1.6	1.7	11	
fmo-3	Y39A1A.19	Xen/Str [9,24]			1.9	2.5	2.0		2.4
lys-4	F58B3.1	Metal [60]					0.4		0.3
nlp-25	Y43F8C.1	Metal [35]				2.4	2.2		
nlp-27	B0213.2	Imm [83]					2.1		2.6
nlp-29	B0213.4	Imm [39,47,84]			3.1	3.1	2.9	7.0	4.0
nlp-30	B0213.5	Imm [41]			2.1	1.9	2.2		3.0
nlp-31	B0213.6	Imm [39,41]			2.1	2.4	2.7	1.8	3.6
oac-46	T14D7.2	–			1.6	2.0	1.7		2.0
phi-59	T19B10.2	Imm [41], Xen/Str [20]			2.2	3.0	2.6	2.2	3.0
pho-6	F52E1.8	Metal [35], Endo/Lyso [3]				2.1	2.3		4.6
ptr-8	F44F4.4	–			2.0	2.5	1.9		2.2
scl-24	F08E10.7	Xen/Str [78]				0.5			0.6
spe-11	F48C1.7	Metal [35], Xen/Str [76]				2.3	2.6		4.8
sqrd-1	F02H6.5	Mitoc [9]				0.5	0.6		0.6
thn-1	F28D1.3	Imm [2,29]					0.5		0.5
ttr-29	R90.4	–					1.8	5.3	2.7
ttr-8	R13A5.6	–				2.2	2.4	1.6	2.9
	C14A6.16	–	1.8	1.5	2.3	4.8	2.9	5.1	3.7
	C30F12.3	–				1.6	2.2		3.1
	D1086.9	–					3.7		8.9
	F07B7.8	–				6.1	4.1		12
	F13D12.3	–				2.1	1.5	1.6	1.9
	F16B4.7	–				2.4	1.7		2.5
	F21H7.3	–				2.1	1.6		1.8
	F26G1.2	Xen/Str [71]				2.0	1.9		2.1
	F41C3.2	–			1.6	2.0			
	F45D11.14	–				0.4	0.6	0.4	0.4
	F52F10.2	Endo/Lyso [9,24]				2.2	1.6		2.0
	F56D3.1	Xen/Str [22]				2.2	1.5		2.4
	H39E23.3	–				5.1	5.8		9.4
	K11G9.5	Xen/Str [14], IonT(−) [9]			2.1	1.9	1.9		1.6
	M162.5	Metal [35]			1.7	3.1	2.2	2.6	2.7
	T28D6.3	Metal [35], Xen/Str [30]				0.4		0.2	0.6
	Y43C5A.3	Imm [29], Metal [35]	1.6	1.5	1.8	3.5	3.3	2.7	4.5
	ZK970.7	Imm [29], Metal [35]	1.9	1.5	5.9	10	7.0	29	11

Table 3 (*Continued*)

Gene		Category	Fold Δ 20nmAgNP					Fold Δ Ag^+	
Name	Sequence		#1 4 h	#2 4 h	#1 8 h	#1 24 h	#2 24 h	#2 4 h	#2 24 h
Sustained response to 20nmAgCit									
amt-1	C05E11.4	Imm [29], IonT(+) [9]	0.6		0.6	0.5	0.6		
clec-74	Y46C8AL.8	Imm [29], Xen/Str [76]	1.7	1.9		2.0			2.0
clec-9	Y70C5C.2	Metal [33,35]	3.1	2.4	3.0	2.0	1.7		1.8
cyp-32A1	C26F1.2	Imm [29]	1.7	1.8	1.8	2.0	1.9	4.5	2.2
ech-9	F01G10.3	Imm [29,65], Lipid [48], Perox [9]	1.8	2.4	1.8		1.5	6.6	
hmit-1.1	Y51A2D.4	IonT(+) [9]	2.2	2.4	2.3	2.0			0.5
ora-1	F57H12.3	–	29	12	16	20	8.8	58	18
vglu-3	T07A5.3	Xen/Str [20]		1.7	1.6	2.0	1.6		1.9
	C15A11.7	Imm [29,65]	1.6	2.0	2.5	2.5	1.9		1.9
	C34F11.8	Imm [29,41,65]	1.7		1.8	1.8	1.9	5.4	2.1
	C49C3.9	Imm [2,29]	1.5	2.5	2.0	1.5	1.7	4.5	2.0
	F59E11.7	–	2.2	1.6	2.1	2.4	2.2	9.2	3.2
	R08E5.3	Imm [65], Metal [35]	0.5	0.4	0.7		0.6		0.6
	T03F7.7	–	1.6			2.0	1.6	4.1	2.2
	T13F3.6	Imm [29], Metal [35], Xen/Str [30]	0.6	0.6	0.6	0.5	0.7	0.3	
	ZK673.1	Imm [29]		0.5	0.6		0.6	0.4	0.5

Microarray data indicating differential gene regulation in response to 100 μg/mL 20nmAgCit or 12.5 μg/mL Ag^+ for indicated times was compared to published expression/function information in order to assign genes into general response categories. Categories: immune response (Imm), metal response (Metal), xenobiotic or heat stress (Xen/Str), lipid metabolism (Lipid), endosome or lysosome associated (Endo/Lyso), mitochondrial (Mitoc), peroxisomal (Perox), dietary restriction (DR), cation transport (Ion(+)), anion transport (Ion(−)). For genes regulated up for some exposures and down for others, ↑ or ↓indicates category for up or down regulation only. Genes listed in table are limited to those that had fold changes in response to 20nmAgCit ≥ 2 fold, and/or to Ag^+ ≥ 5 fold in at least one experiment at any assessed exposure time.

20nmAgCit exposure. Functional annotation of these genes using the Database for Annotation, Visualization and Integrated Discovery (DAVID [47,48]) or Ingenuity Pathway Analysis (IPA™, QIAGEN, www.qiagen.com/ingenuity) did not return significantly enriched functional groups or clusters. Based on published information on gene function and expression data accessed from WormBase [44], OMIM [49], and Google Scholar [50] however, 85 of those genes could be assigned to one or more general response categories. Comparing our results to published gene expression data sets, we found many alternately regulated genes in common with *C. elegans* response to infection, including *Microbacterium nematophilum* [51], *Pseudomonas aeruginosa* [52,53], *Drechmeria coniospora* [43], *Leucobacter chromiireducens* [54], *Candida albicans* [55], *Vibrio cholerae* [56], and other pathogens [57]. Genes that were included in the 20nmAgCit general metal response category included those that were differentially regulated in the same direction as by mercury [58], cadmium [59,60], and/or arsenic [61,62]. Gene regulation in the same direction as in response to oxidative stress [63,64], heat shock [65], ethanol [66], organophosphates [62,67–69] and other xenobiotics including glucose [70–72], was combined together into a single category, Xen/Str. It is important to note that communalities found by comparing expression results in this manner are likely to detect downstream as opposed to primary effects for each category.

Of 46 genes differentially regulated in *C. elegans* by exposure to 100 μg/mL 20nmAgCit in the same direction as in response to infection, 24% were more highly regulated after 4 h of exposure than for later time points, while 46% showed increasing regulation over 24 h, again indicating that the immune response to AgNP tends to increase over time (Fig. 3). 25 genes were regulated in the same direction as in response to metals, and of those, 72% were early responders, while only 24% showed increased regulation at later time points. Thus, as when looking at individual genes with specific known functions, more general immune responses also increased while metal response decreased over the 24 h assessment period. Xen/Str type gene regulation also showed an early type response; of 29 genes identified, 66% peaked early, 34% peaked late, and none fell into the steady or 8 h only categories (Fig. 3).

Many viruses have diameters in the 20–30 nm range [73–75], and in mice vaccines with 40 nm polystyrene carrier beads can induce immune responses without adjuvants [76], indicating that the immune response we observed could have been due to particle size alone. We therefore repeated microarray analysis on *C. elegans* adults exposed to 20nmAgCit for 4 or 24 h, this time using citrate coated 20 nm gold spheres (20nmAuNP) as a control for particle size, and Ag^+ as a control for silver exposure. In order to determine an appropriate Ag^+ dose for comparison to 100 μg/mL 20nmAgCit, we tested adult *C. elegans* for changes in motility and morphology in response to Ag^+. Using a WMicrotracker, we found a slight initial peak of activity at 2 h of exposure to 20nmAgCit at the 100 μg/mL dose, followed by a slight dip in motility beginning at 4 h of exposure corresponding to an average decrease of just over 20% from the 5 h point on (Fig. 4A). In contrast, exposure to 25, 50, or 100 μg/mL Ag^+ was associated with a 50–60% jump in activity at 1 h of exposure followed by a drop (Fig. 4B), a pattern we have observed in response to other metal ions (manuscript in preparation). Exposure to 12.5 μg/mL Ag^+ produced the most similar motility pattern to that of 100 μg/mL 20nmAgCit. By light microscopy, adult *C. elegans* exposed to 100 μg/mL 20nmAgCit for 24 h

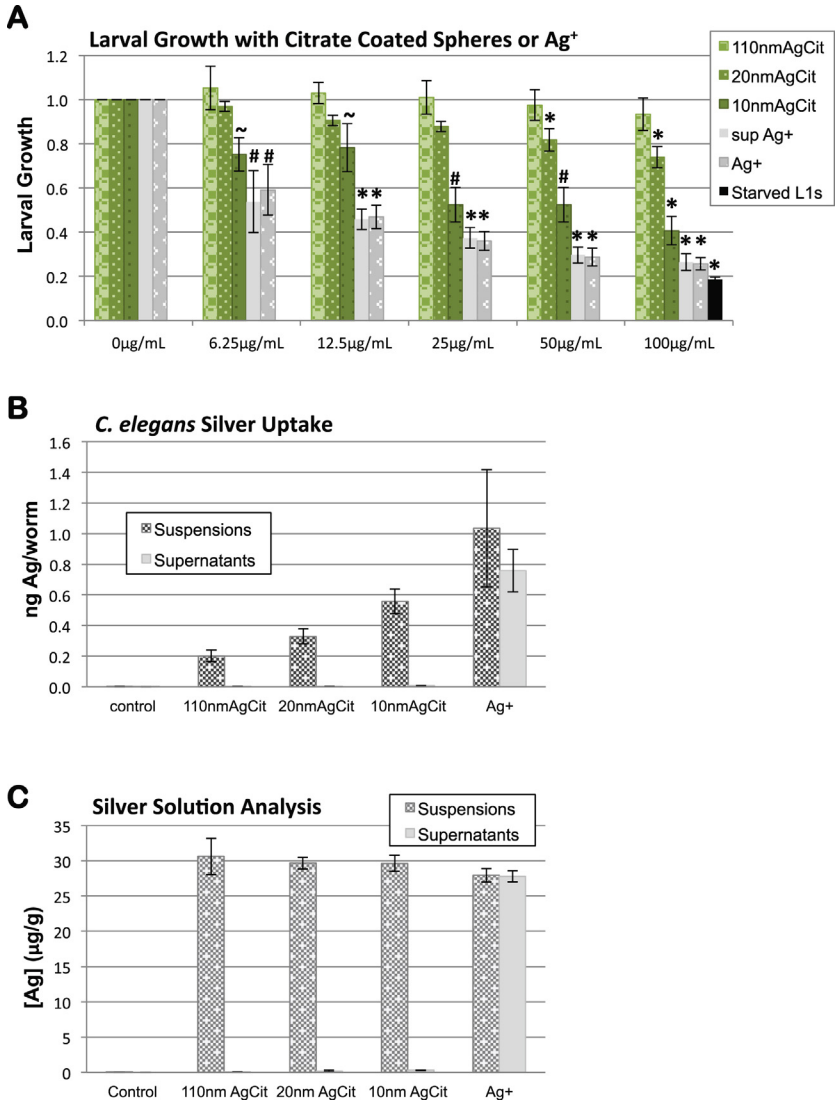

Fig. 2. For citrate coated nanospheres, decreasing size correlates with increasing uptake and toxicity. (A) Synchronized *C. elegans* larvae exposed for 3 days to AgNP spheres or Ag+ at the indicated concentrations were assessed by COPAS for growth. COPAS assessed larval length was standardized to controls and presented as the mean ± SD among three to six separate trials. Student's *t*-test *p*-values are all <0.05 for comparisons among the 3 AgNP sizes at concentrations of 25 μg/mL and above, and <0.01 comparing Ag+ to AgNPs at concentrations of 12.5 μg/mL and above. High-speed supernatants of all silver suspensions were also tested (see Supp. Fig. 1), that of Ag+ (sup Ag+) shown here. Student's *t*-test *p*-values relative to water controls <0.05 (~), <0.01 (#), <0.001 (*). (B) *C. elegans* adults exposed for 1 day to suspensions or high-speed supernatants of AgNP spheres or Ag+ at 25 μg/mL were assessed by ICP-MS for organismal silver uptake. (C) Silver suspensions and high-speed supernatants were assessed for silver concentration by ICP-MS.

did not appear to have altered morphology (Fig. 5A and B). In contrast, those exposed for one day to 100 μg/mL Ag^+ had fewer internal eggs, thinner intestines, and general morphology resembling very old worms (Fig. 5C). For Ag^+, the highest concentration at which morphological changes were not observed was 12.5 μg/mL (Fig. 5D). We therefore selected 12.5 μg/mL Ag^+ for use as a control for exposure to 100 μg/mL 20nmAgCit for microarray analysis.

20nmAuNP at 100 μg/mL induced differential regulation in only three genes at 4 h exposure (*gst-19* down 1.6-fold, *nspe-1* up 1.8-fold, and *T23G11.4* down 1.5-fold) and two genes at 24 h (*asp-10* down 2.2-fold, and *R08E5.3* down 1.5-fold), indicating that the responses to 20nmAgCit were not due to particle size or concentration. Comparing the response at 4 h exposure to the two forms of silver, 123 genes were significantly differentially regulated by 20nmAgCit in this second microarray assessment vs. 792 for Ag^+, more than 6 times the number of genes at 1/8th the dose. Of the genes differentially regulated by 20nmAgCit at 4 h, 81 genes or 67% were also differentially regulated by Ag^+ (Fig. 6A). At 24 h, the difference between the two conditions was less extreme, with 88 genes being differentially regulated by 20nmAgCit exposure vs. 183 for Ag^+ and 79 in both, though many more genes were still differentially regulated by Ag^+ than by 20nmAgCit.

Table 4
Ingenuity networks.

ID	Molecules in network	Score	#	Top functions
4 h Ag^+ exposure				
1	↑ **ABCB6**, ↑ **ABCB9**, ↓ **ACOT8**, ↓ **ATP6V0B**, ↓ **ATP6V0C**, ↓ **ATP6V1A**, ↓ **ATP6V1B1**, ↓ **ATP6V1D**, ↓ **ATP6V1E1**, ↓ **ATP6V1G1**, ↓ **ATP6V1H**, ↑ **CAT**, ↑ **CTSZ**, ↑ **DCXR**, ↑ **DPP4**, ERK1/2, ↑ **FAAH**, ↑ **GALNT2**, ↑ **GBA**, glutathione peroxidase, glutathione transferase, ↓ **GSTK1**, ↑ **GSTO1**, H^+-exporting ATPase, H^+-transporting two-sector ATPase, ↑ **HPGDS**, ↓ **ICMT**, IL12 (complex), Ldh (complex), ↑ **LMNB2**, PXR ligand-PXR-Retinoic acid-RXRα, Secretase gamma, Sos, ↑ **STX1A**, Vacuolar H+ ATPase	48	24	Molecular transport, infectious disease, nucleic acid metabolism
2	26s Proteasome, ↓ **AACS**, ↑ **ABCD3**, ↓ **ACOX1**, ↑ **ACSL4**, Akt, AMPK, Calcineurin protein(s), ↓ **CLN3**, ↑ **CPE**, ↑ **CYP2J2**, cytochrome C, cytochrome-c oxidase, ↑ **DUSP14**, FSH, ↑ **GGT1**, ↑ **HSD17B4**, ↓ **IDH1**, IgG, IL1, Insulin, ↑ **KCNQ1**, Lh, ↑ **MYH10**, ↑ **PLA2G6**, PRKAA, Proinsulin, ↓ **Scd2**, ↓ **SELENBP1**, ↓ **SIRT4**, ↓ **SLC15A1**, ↑ **SLCO2B1**, ↓ **SOD1**, ↑ **STIM1**, ↑ **UGCG**	40	22	Lipid metabolism, small molecule biochemistry, energy production
3	↓ **ABCB1**, ↑ **ABCC1**, ↓ **ALDH9A1**, ↓ **AMT**, ↑ **ANXA7**, ↓ **BCAT1**, caspase, ↑ **CC2D1A**, CD3, Cg, Ck2, Collagen(s), Creb, ↑ **CROT**, ↓ **GCH1**, ↓ **GCSH**, ↓ **GLDC**, Histone h3, Histone h4, Hsp27, Hsp70, Hsp90, LDL, ↑ **LIPA**, ↓ **MPC1**, NFkB (complex), P38 MAPK, ↑ **PDCD6IP**, Pkc(s), ↑ **SF3B2**, ↑ **SLC26A5**, ↑ **TOM1L2**, trypsin, Ubiquitin, Vegf	30	17	Developmental disorder, hereditary disorder, metabolic disease
4	↑ **ABCA3**, ACAD10, ↓ **ACADSB**, ↑ **ALKBH4**, ATP10D, ATP11A, ATP11B, ATP11C, ATP8A1, ATP8B1, ↑ **ATP8B2**, ↓ **CEPT1**, ↑ **CRIP1**, DNAJC2, DTX2, FKBP10, ↑ **GHITM**, ISCU, ↑ **KRI1**, LIN37, LIN54, NFXL1, ↑ **NNT**, PIGG, PIGO, PLD3, ↓ **PLD4**, ↓ **SLC16A10**, ↑ **TMEM30A**, ↑ **TMLHE**, ↓ **TMX1***, ↓ **TXNDC12***, UBC, USP19, VOPP1	26	15	Lipid metabolism, molecular transport, small molecule biochemistry
5	A1BG, ↑ **ABCB9**, ↓ **ACMSD**, ↑ **COX3**, ↓ **ADHFE1**, ↓ **AGXT2**, ALOX15B, ↓ **AQP8**, AR, C21orf33/LOC102724023, ↓ **CA7**, ↑ **Ces1c**, Cyp2d9 (includes others), CYP3A, ↑ **CYP3A7-CYP3AP1**, ↑ **CYP4V2**, CYP7B1, ↓ **HAAO**, HDL-cholesterol, HNF4A, ↓ **HPRT1**, ↓ **KDM8**, LAD1, LIPC, LPCAT3, LYPLA2, MGST1, MSMB, NAT8, NR1I2, ↑ **OSBPL8**, protoporphyrin IX, ↓ **SORD**, TCF19, TNF	26	15	Small molecule biochemistry, gastrointestinal disease, hepatic system disease
6	↓ **ACOT8**, ↓ **ATP13A3**, ↑ **BROX**, ↑ **C10orf118**, CCDC124, CHMP4B, CHTOP, ↑ **DHRS1**, DIAPH3, ERG, FMNL2, FMNL3, GAK, GMFB, HPCAL1, ↓ **HYI**, ↑ **MAK16**, MT1A, ↓ **MTFP1**, MYO1D, ORC6, PARVA, ↑ **PLCXD2**, PLEK, PLEKHA5, RAB2A, ↑ **RASGEF1B**, RHOBTB1, RYR3, SIRT5, ↓ **SLC39A13**, ↓ **SLC8B1**, ↑ **SPTBN5**, ↑ **TTC36**, UBC	23	14	Connective tissue disorders, derma. Diseases and conditions, dev. disorder
7	↓ **AMD1**, ARHGEF9, ↑ **ARHGEF16**, beta-estradiol, ↑ **BICC1**, ↑ **CAPN8**, ↓ **CHRNA6**, CHRNB3, ↓ **CMPK1**, ↓ **DNAJC3**, DNAJC4, ↓ **ECHS1**, EGFR, ERBB4, ↑ **GLRA1**, ↑ **GLRA3**, GLRA4, GLRB, Hba, Hba1/Hba2, hemoglobin, ↑ **LGMN**, LRIG1, ↑ **LRIG3**, ↑ **MCTP1**, miR-382-5p (miRNAs w/seed AAGUUGU), NME3, NRG (family), SCARB1, TMC4, ↑ **TMCO4**, TMEM245, UROD, VIM, YWHAZ	22	14	Neurological Disease, protein synthesis, immunological disease
8	AIDA, ANGPTL7, ↑ **APP**, ↑ **BMPR1B**, Calmodulin, CCNL1, ↑ **CDO1**, Collagen type I, ERK, ↑ **ETNPPL**, FAM189B, ↑ **FBLN1**, ↑ **FBXL20**, FOXS1, ↓ **GALE**, ↑ **GPKOW**, Immunoglobulin, Jnk, LRRTM3, Mapk, ↓ **MAT2A**, MAT2B, NAGA, NECAB1, PATL1, PDGF BB, Pka, POMZP3, ↓ **PTDSS1**, Rac, ↑ **RRS1**, TCR, ↓ **TMEM53**, TMX3, ↑ **WWOX**	20	13	Amino acid metabolism, nucleic acid metabolism, small molecule biochemistry
9	↓ **AASDHPPT**, BCL2, CISD2, ↑ **COMTD1**, CPOX, ↑ **CTSF**, Cyp2d9 (includes others), ELAVL1, EPHX1, FMO, ↑ **FMO5***, ↑ **Fmo9***, FUCA1, ↑ **GART**, IKBIP, LEP, miR-296-5p (miRNAs w/seed GGGCCCC), MPV17L, NAPG, Ncoa-Nr1i2-Rxra, NMT2, NUSAP1, ↑ **OPLAH**, ↑ **OSBP2**, PAXIP1, ↑ **SLC37A3**, ↑ **SLC50A1**, ↓ **SPNS1**, ↑ **SPTLC2**, SPTSSA, TCN2, TMEM97, TP53, UBL3, UPF2	18	12	Molecular transport, cellular assembly and organization, cancer

Table 4 (*Continued*)

ID	Molecules in network	Score	#	Top functions
10	AQP1, ↓ **AQP8**, betaine, CALML3, CD68, ↑ **CD109**, CDC7, CHD4, CST3, DPYSL3, FCGR3A/FCGR3B, GSTA5, GTPBP1, HADH, HLA-DQA1, HLA-DRA, HPGD, ↓ **HSD17B8**, HSD17B10, HSPB2, hydrogen peroxide, lipid peroxide, mevalonic acid, ↑ **MIOX**, NFAT5, NNMT, PPP1R3C, RAD21, RORC, ↓ **SELENBP1**, SFTPB, SLC20A1, ↓ **SLC7A2**, SMPD2, TGFB1	8	6	Cell morphology, connective tissue development and function, organ morphology
24 h Ag^+ exposure				
1	↑ **ABCB6**, ↑ **ACE2**, ↑ **ACOX1**, ↑ **ACPP***, ↓ **ACY1**, ALAD, ANKRD17, CFTR, CPOX, CYP3A5, Cyp3a25 (includes others), CYP4F12, ↑ **CYP4V2**, ↓ **DNASE2B**, FAH, FAM214A, ↑ **FMO5**, ↑ **GBA**, GFRA1, HAL, HPD, IMPACT, KRT23, ↓ **LMNB2**, ↑ **NCAM1**, NEK7, NT5C3A, PPOX, PXMP2, SLC25A39, ↓ **SQRDL**, TNF, TRPV2, UBC, ZNF420	34	12	Gastrointestinal disease, hematological disease, hepatic system disease
4 h 20nmAgCit exposure				
1	↓ **ACADSB**, AKR1C4, APP, ↑ **ATP8B2**, CBR4, ↑ **COMTD1**, CSTB, ↑ **CYP4V2**, DNAJC2, EPHX1, FKBP10, ↑ **FMO5**, HAGH, HMBS, HSD17B4, ↓ **HSD17B8**, ↑ **LRRC58**, LYN, MAPK8, MFGE8, progesterone, PTGDS, QPCT, RAD21, SCGB1A1, ↑ **SERPINB3**, SERPINB4, ↓ **TMEM53**, TRIB1, TRMT2A, TXNDC5, ↓ **TXNDC12**, UBC, UPF2, ZNF420	25	10	Endocrine system dev. and function, small molecule biochemistry, lipid metabolism
2	↑ **ABCB6**, ↑ **ACOX1**, ADIPOR2, ALAD, CPOX, CYP4F12, ESR1, FAH, FAM214A, HAGH, HAL, HMBS, HPD, ↑ **HPGDS***, IMPACT, Kap, KRT23, LPCAT3, MLF2, NT5C3A, ↓ **P4HA1***, P4HA2, ↑ **PON3**, PPOX, PXMP2, QPCT, RAD51B, SLC25A39, SLC4A4, TGFB1, TRPV2, TXNRD2, UBC, UGT8, UROD	11	5	Hematological disease, metabolic disease, gastrointestinal disease
24 h 20nmAgCit exposure				
1	↑ **ACPP,** adenosine, ANKRD17, beta-estradiol, CFTR, Cyp2d9 (includes others), CYP3A5, ↑ **CYP4V2**, EPHX1, ↑ **FMO5**, FOLR1, FSHR, ↑ **GBA**, HSD11B1, HSPA4, NCOR1, NEK7, NPR1, NR1I2, PGRMC1, PSAP, PTPRE, PTPRJ, SASH1, SCARB2, SHBG, SIAH2, SIN3A, SNAPIN, SOD2, ↓ **SQRDL**, STIP1, TCP1, UBC, ZNF420	14	5	Lipid metabolism, molecular transport, small molecule biochemistry

Networks of human genes are listed, with differentially regulated *C. elegans* homologs in bold, red arrows indicate up regulation, green arrows indicate down regulation in response to 100 μg/mL 20nmAgCit or 12.5 μg/mL Ag^+ for indicated periods.

Comparative analysis of the differentially expressed genes using DAVID highlighted the toxicity of Ag^+ relative to 20nmAgCit. Using thresholds of count >4 and EASE score (modified Fisher Exact *p*-value) < 0.05, the list of genes differentially regulated by Ag^+ at 4 h of exposure identified 28 GO terms, while only one GO term each was associated with exposure to 4 h 20nmAgCit or 24 h Ag^+, and no GO terms were associated with 24 h 20nmAgCit exposure. For 4 h Ag^+ exposure, GO term categories with the most genes in them were carboxylic acid metabolic process and cation transport with 26 genes each, while 23 genes fell in within the positive regulation of organism growth, 18 in nucleic acid biosynthetic process, 17 in lipid metabolic process, 8 in cell redox homeostasis, and 5 in catechol metabolic process GO terms (Fig. 6B). The only GO term associated with 4 h 20nmAgCit exposure was lipid modification with 4 genes. The only GO term associated with 24 h Ag^+ exposure was protolysis with 12 genes. Similarly, Ingenuity Pathway Analysis (IPA) identified 10, 1, 2 and 1 networks with 5 or more genes each for Ag^+ at 4 h, Ag^+ at 24 h, 20nmAgCit at 4 h, and 20nmAgCit at 24 h, respectively (Table 4). The most complete network identified is that for "Molecular Transport, Infectious Disease, Nucleic Acid Metabolism" for 4 h Ag^+ exposure, with 24 genes and an IPA score of 48 (Fig. 6C). Differential expression within this network includes the down regulation of a group of 9 *C. elegans* homologs of human lysosomal proton pumps, none of which are differentially regulated by AgNP. This down regulation is likely due to accumulation of Ag^+ in lysosomes.

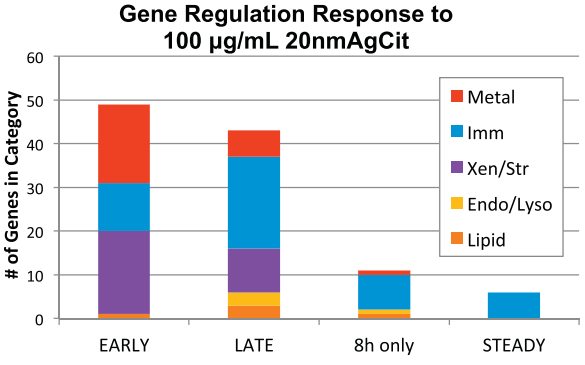

Fig. 3. Effects of 20nmAgCit on gene expression. Synchronized adult *C. elegans* were exposed to 100 μg/mL 20nmAgCit for 4, 8, or 24 h and assessed by microarray for altered gene expression. Metal response gene regulation decreased over the assessed time period, while innate immune response gene regulation held steady or increased.

In this second microarray experiment, the CNC and NLP genes (with the exception of early responding *nlp-26*) were

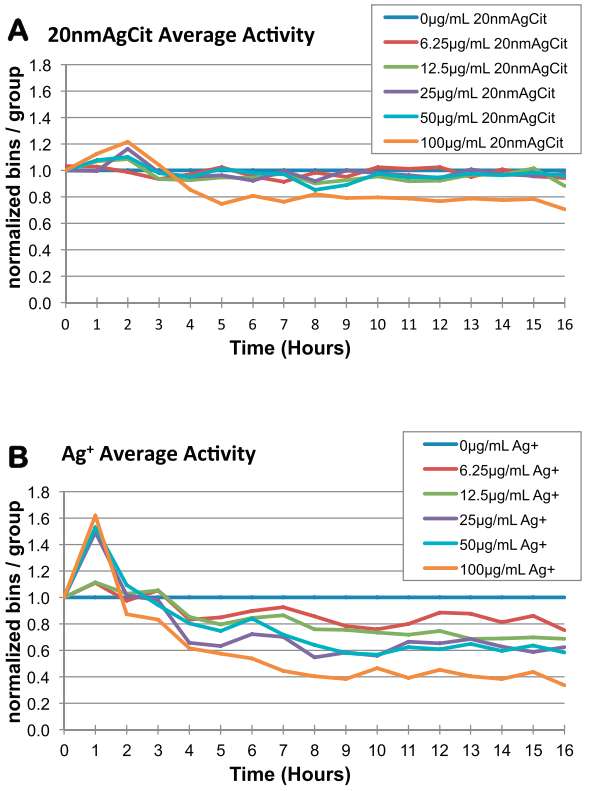

Fig. 4. Effects of 20nmAgCit and Ag+ on motility. (A) Group motility assessment of adult *C. elegans* exposed to 20nmAgCit. (B) Group motility assessment of adult *C. elegans* exposed to Ag+.

again more highly up regulated at the later time point with 20nmAgCit exposure, and with the exception of *cnc-3* (up for 20nmAgCit 1.7-fold at 24 h in experiment #2 only), they were up regulated to a greater extent with Ag^+, though the timing of regulation in response to Ag^+ was varied (Table 3). Fungal response genes *fip-1*, *fip-5*, and *fipr-26* were again up regulated at 24 h but not 4 h in response to 20nmAgCit, and here too the timing of the response to Ag^+ exposure was more variable. Metal response genes *hmt-1*, *ftn-1*, and *numr-1* were up regulated to similar extents with exposure to 20nmAgCit as in the first experiment, and were also up regulated with 4 h exposure to Ag^+ by 5.8, 13, and 81-fold, respectively. Metal response genes *mtl-1*, *mtl-2*, and *cdr-4* were differentially regulated by Ag^+, but not by 20nmAgCit. Additionally, *C14H10.1* (a *C. elegans* gene with significant homology to human zinc transporter ZIP13 [44]), was down 1.6-fold at 4 h but not 24 h in response to Ag^+ only. Catechol-O-methyltransferases (COMT) are involved in the inactivation of neurotransmitters and other substrates. *C. elegans* homologs *comt-3* and *comt-4* also showed an early response to AgNP, and higher levels of up regulation with Ag^+.

Looking at the gene regulation response to Ag^+, the magnitude of gene regulation in response to Ag^+ was much higher at 4 h relative to 24 h exposure, and in contrast to 20nmAgCit, the only category of gene response that was significantly different between the two time points was an increase in regulation of lysosome associated genes at 24 h (data not shown). Innate immune response genes *fipr-22*, *fipr-23*, and *C50F7.5* had increases in expression of 10-fold or more with Ag^+ exposure, but were not differentially regulated with 20nmAgCit. Many stress response genes, including *ctl-1*, *ctl-2*, *hsp-16.1*, *gst-2*, *gst-22*, *gst-26*, *gst-27*, *gst-28*, *gst-29*, *sod-1*, and *vit-1* were differentially regulated with Ag^+ but not with 20nmAgCit exposure. Similarly, 13 UGT genes (*ugt-1*, *ugt-2*, *ugt-5*, *ugt-10*, *ugt-11*, *ugt-22*, *ugt-26*, *ugt-39*, *ugt-44*, *ugt-46*, *ugt-48*, *ugt-54*, and *ugt-63*) were all differentially regulated by Ag^+ at the 4 h time point only, and did not show altered regulation in response to 20nmAgCit. Additionally, *ugt-3*, which showed 6.8 and 4.1-fold increases in response to 4 h 20nmAgCit exposure in experiments 1 and 2, respectively, was up regulated 84-fold in response to 4 h Ag^+ exposure (Table 3). Neuronal genes differentially regulated only by Ag^+ and only at 4 h included *cat-4*, *ncs-3*, *rig-5*, and *zip-5*. Genes involved in DNA stabilization or synthesis up regulated by 4 h Ag^+ only included the histone genes *his-10* and *his-11*, as well as *C23H4.6* (a close homolog to human Structural Maintenance of Chromosomes Protein 6) and *F38B6.4* (involved in the purine biosynthetic pathway). Cation transport genes differentially regulated by Ag^+ but not 20nmAgCit exposure included *mps-2*, *catp-5*, *B0454.6*, *ncx-7*, and *cng-1* which were down regulated at 4 h, while *F53A9.8* was up at 4 h but down at 24 h, indicating a general down regulation of cation transport. The expression of genes associated with anion transport including *glc-1*, *glc-2*, *F21G4.1*, *mrp-2*, and *sulp-5*, were all increased with Ag^+ exposure at 4 h, while *C35A5.3* was down at 4 h and *best-7* was down at 24 h, consistent with a trend toward up regulation of anion transport.

3.4. Effect of coat and shape on nanosilver toxicity

For evaluation of the effects of coat and charge on AgNP toxicity, we selected two sizes of silver nanospheres with three different coatings for further study. *C. elegans* larvae were exposed for 3 days to silver spheres of 20 nm diameter coated in branched polyethyleneimine (20nmAgBPEI), polyvinylpyrrolidone (20nmAgPVP), or polyethylene glycol (20nmAgPEG) at concentrations of 6.25–100 µg/mL in axenic nutrient media. Length of *C. elegans* exposed to 20nmAgPEG at 6.25 µg/mL was at $72 \pm 8\%$ ($p < 0.01$, $n = 4$) of controls, and 20nmAgPEG exposed worms were the smallest at each of the higher concentrations as well (Fig. 7A). Therefore, of the four coats tested, PEG imparts the highest toxicity to 20 nm silver spheres. While there was a small yet significant reduction in larval growth at 25 µg/mL for 20nmAgPVP, but not for 20nmAgBPEI, the difference between these two was not significant at any concentration. A complicating factor for assessment of relative BPEI coat toxicity is that at 125 µg/mL BPEI, the concentration estimated to be present on the surface of washed 20nmAgBPEI at 100 µg/mL, the length of *C. elegans* was at $70 \pm 6\%$ ($p < 0.05$, $n = 3$) of matched controls, while the other coat compounds did not reduce larval growth (Supp. Fig. 1A). Therefore, part of the toxicity of 20nmAgBPEI may be due to BPEI itself. However, high-speed supernatants prepared from the 20 nm AgNP suspensions to assess the

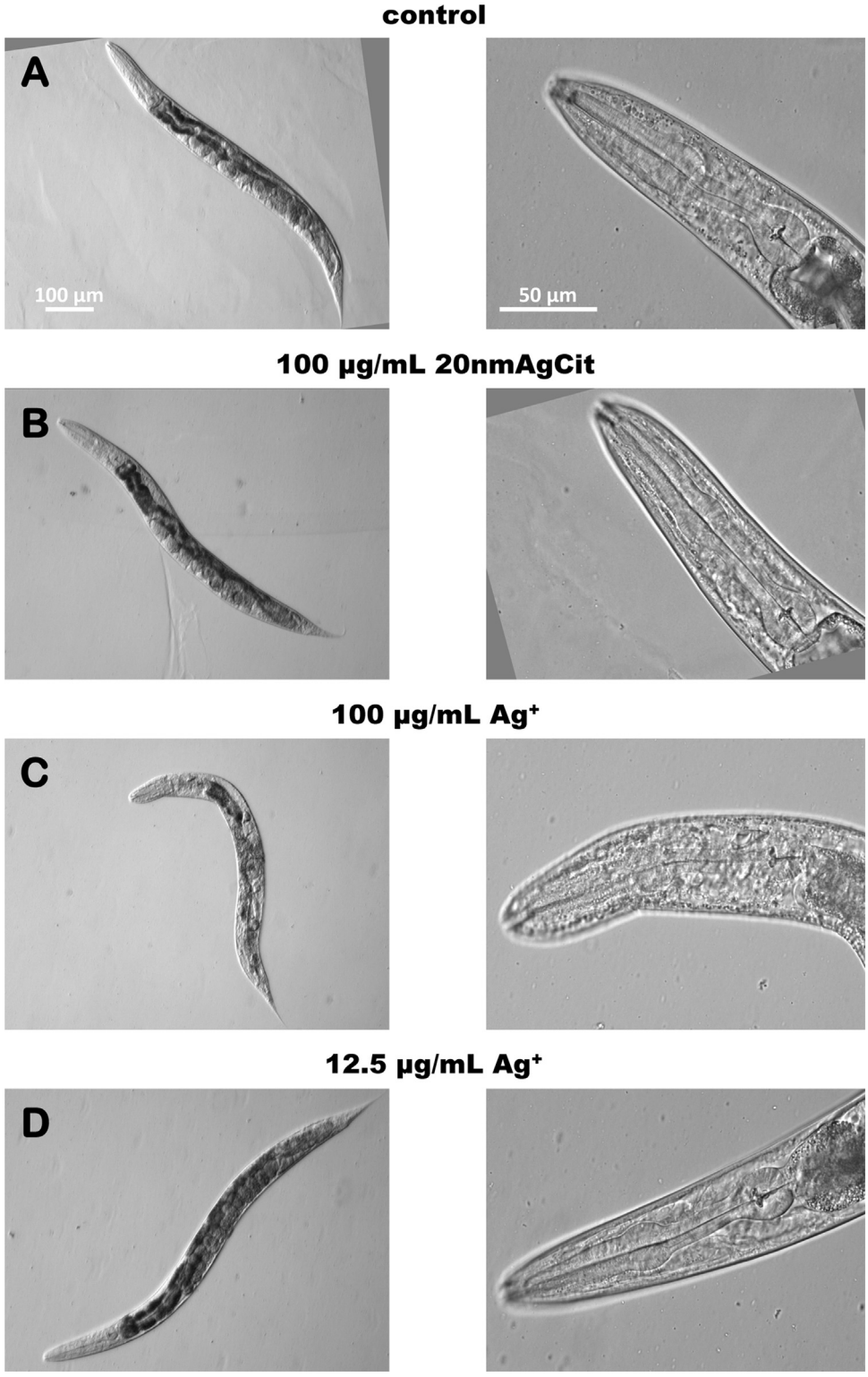

Fig. 5. Adult morphology. Micropictographs using oblique illumination of adult *C. elegans* exposed for 1 day to indicate silver suspensions or water control. The left column shows representative *C. elegans* images taken with a 10× objective. The right column shows the head of the same worm as in the left column taken with a 40× objective.

toxicity of the AgNP solution soluble fraction did not reduce growth significantly (Supp. Fig. 1B and C), indicating that toxic levels of BPEI were not released from the surface of 20nmAgBPEI in solution prior to dosing. For 20nmAgPEG, 20nmAgPVP, and 20nmAgBPEI at 100 μg/mL, *C. elegans* length was at 43 ± 5% ($p < 0.001$, $n = 4$), 51 ± 10% ($p < 0.001$, $n = 6$), and 54 ± 3% ($p < 0.01$, $n = 3$), respectively. Student's *t*-test *p*-values for the difference at 100 μg/mL between these each of these three species and 20nmAgCit was <0.01, indicating that citrate is the least toxic of the four tested coats.

We also assessed the toxicity of 110 nm diameter silver spheres coated in PVP (110nmAgPVP) or PEG (110nmAgPEG). BPEI coated 110 nm sliver spheres were not tested due to technical difficulties. After 3 days of exposure to 100 μg/mL AgNP in CeHM, *C. elegans* length was at 72 ± 9% ($p < 0.01$, $n = 5$) for 110nmAgPEG, and 77 ± 8% ($p < 0.05$, $n = 4$) for 110nmAgPVP (Fig. 7B). The differences between the toxicity of the PVP and PEG coats for these larger AgNP spheres was not significant at any concentration, but Student's *t*-test *p*-values for the differences between these two and 110nmAgCit at 100 μg/mL was <0.05, indicating again that for AgNP coats, citrate is better tolerated than PVP or PEG. Comparing larval length at 100 μg/mL between 20 nm spheres and 110 nm spheres with a given coat gives *p*-values of <0.05 for citrate and <0.01 for PVP or PEG, indicating that when comparing silver mass equivalents, smaller AgNP spheres with a given coat are more toxic than larger ones.

In order to assess the effect of shape on AgNP toxicity, we exposed *C. elegans* larvae to nanosilver plates in two size ranges. Larval growth of *C. elegans* exposed to 550rAgPlates at 6.25 μg/mL was at 80 ± 7% ($p < 0.01$, $n = 5$) of controls, and reduced steadily as concentration increased, to 48 ± 10% ($p < 0.001$, $n = 5$) at 100 μg/mL (Fig. 7C), putting the relative mass based toxicity of 550rAgPlates similar to that of that of 20nmAgPEG. 1100rAgPlates reduced growth to a lesser extent, with length at 74 ± 6% ($p < 0.001$, $n = 6$) at 100 μg/mL, putting the toxicity of 1100rAgPlates as roughly equivalent to that of 110nmAgPEG. Thus, for AgNP plates as well as spheres, decreasing size correlates with increasing toxicity.

Looking at silver uptake vs. toxicity for 20 nm silver spheres, the toxicity ranking of 20nmAgPEG > 20nmAgPVP > 20nmAgCit is matched by decreasing silver uptake of 0.76, 0.46, and 0.33 ng/worm, respectively (Fig. 2B and 8). The exception to this trend is 20nmAgBPEI, with toxicity similar to that of 20nmAgPVP, but silver uptake less than that for 20nmAgCit at 0.23 ng/worm. Thus, when comparing AgNPs with different coats, increased silver uptake does not necessarily correspond to increased toxicity. As with relative toxicity, organismal levels of silver after exposure to 110nmAgPVP or 110nmAgPEG were not statistically different from each other. There was a trend of less silver uptake with 1100rAgPlates relative to that with 550rAgPlates, but not a statistically significant one (Fig. 8). While there was a slight reduction in growth of *C. elegans* exposed to high-speed supernatants of 100 μg/mL 550rAgPlates, with larval length at 86 ± 9% of controls, this did not quite reach our 15% reduction for biological significance (Fig. 7C).

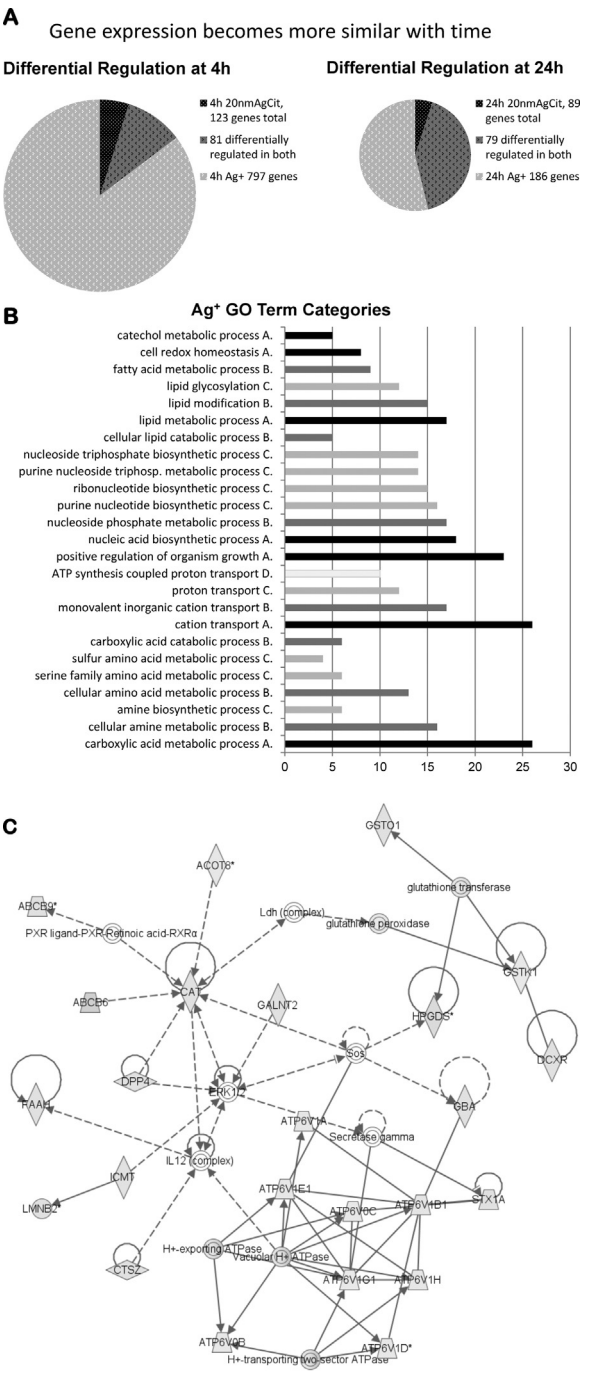

Fig. 6. Gene expression response to 20nmAgCit or Ag^+. (A) Pie charts indicating the total number of differentially regulated genes at 4 and 24 h in response to 20nmAgCit only (black), Ag^+ only (light gray), or both (dark gray). (B) DAVID analysis of Gene Ontology (GO) terms associated with 4 h Ag^+ exposure only. Major categories are shown in black, sub-categories of each are listed above the associated category in sequentially lighter shades of gray. (C) The pathway with the most differentially expressed genes identified by Ingenuity Pathway Analysis in response to 4 h Ag^+ exposure was "Molecular Transport, Infectious Disease, Nucleic Acid Metabolism," with a total of 24 differentially regulated genes.

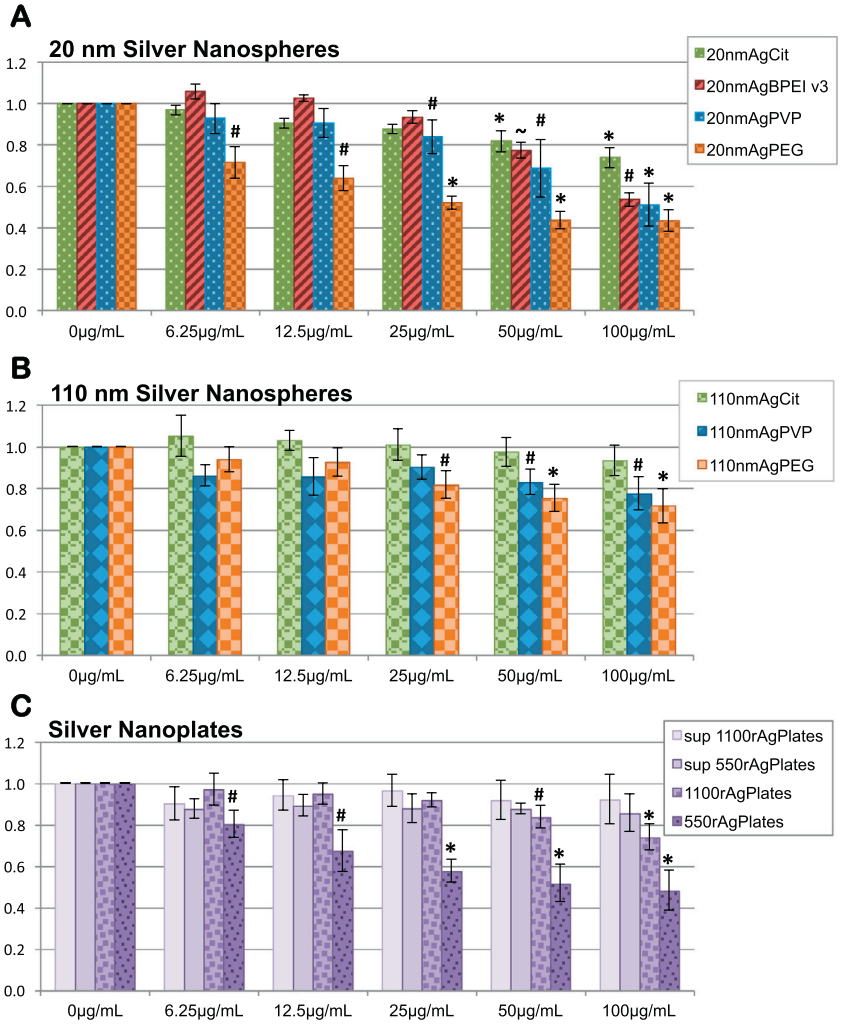

Fig. 7. Effects of coating, size, and shape on nanosilver toxicity. *C. elegans* larvae exposed for 3 days to AgNP of two shapes in two sizes and four different coatings were assessed by COPAS for growth. Student's *t*-test *p*-values <0.05 (~), <0.01 (#), <0.001 (*). (A) For 20 nm silver nanospheres, citrate was the least toxic coat and PEG the most toxic. While the normalized mean length of worms exposed to 20nmAgPVP was slightly less than the mean for those exposed to 20nmAgBPEI at each concentration tested, the difference between the two was not statistically significant. (B) For 110 nm silver spheres, PVP and PEG coatings imparted greater toxicity than citrate. The difference between 110nmAgPVP and 110 nmAgPEG was not statistically significant. (C) Smaller silver nanoplates were more toxic than larger ones. While there was a trend toward reduced growth with exposure to the soluble fraction from 550rAgPlates, it was not significant.

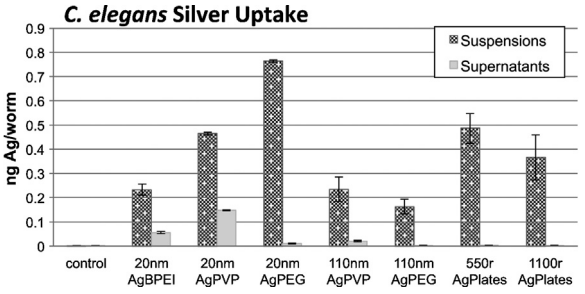

Fig. 8. Silver uptake depends on AgNP size, shape, and coating. *C. elegans* adults exposed for 1 day to indicate AgNP suspensions or high-speed supernatants were assessed by ICP-MS for total silver concentration.

4. Discussion

Given their size, nanoparticles (NP) have the potential to interact with many cellular macromolecules in ways that their component bulk materials cannot. Thus, NP can have unexpected novel beneficial or toxic activities. The antimicrobial activity of nanosilver (AgNP) is especially interesting given growing concerns about the rise of multidrug resistant microorganisms. However, oral exposure to AgNP or ionic silver (Ag^+, which can be released from the surface of AgNP) can retard juvenile rat growth [42,77,78], with Ag^+ exposure resulting in higher levels of tissue deposition and further growth inhibition relative to AgNP exposure [16,42,79]. Size dependent bioactivity of AgNPs has been observed in orally exposed mice, as well as in zebrafish embryos and murine embryonic stem cells,

with smaller AgNPs being associated with increased toxicity [18,19,80]. Using *C. elegans* as an alternative in vivo model for toxicity assessment, we also found that for three sizes of citrate coated silver nanospheres, decreasing AgNP size correlated with increasing toxicity and higher levels of silver uptake, and that relative to AgNP exposure, equimolar Ag^+ from silver acetate was associated with further increases in toxicity and organismal silver uptake.

Gene regulation was assessed in *C. elegans* in response to citrate coated 20 nm silver nanospheres (20nmAgCit) using Ag^+ as a control for silver exposure, but at 1/8th the 20nmAgCit dose to account for the relative toxicity of the two forms of silver. Despite the reduced silver concentration in the dose, Ag^+ induced differential regulation in more than six times the number of genes as AgNP, and many genes regulated by both forms of silver showed far higher levels of regulation with Ag^+ exposure. In contrast, exposure to citrate coated 20 nm gold nanospheres (20nmAuNP) induced low levels of differential regulation in a total of only 5 genes, indicating that nanogold has very little effect on gene expression. Analysis of microarray results indicated that differential regulation of metal response genes tended to peak early with exposure to AgNP, and then decrease over the 24 h assessment period. This may explain why a previous study that assessed gene expression levels in *C. elegans* in response to AgNP, but only after 24 h of exposure, found low levels of regulation in only a few metal response genes [81]. Metal response genes *hmt-1*, *ftn-1*, and *numr-1* were more highly up regulated at 4 h than at 24 h in response to both AgNP and Ag^+, but for each gene levels of up regulation were higher with Ag^+ exposure. Additionally, any more metal specific genes were differentially expressed in response to Ag^+, and the timing appeared more random than in response to AgNP exposure. We also assessed general downstream metal responses by comparing our results to published gene expression data associated with exposure to cadmium, mercury, and arsenic. Here too we found an early pattern of metal response regulation with AgNP exposure, but no clear pattern with Ag^+ exposure.

The largest gene response category activated by AgNP exposure, both for specific genes and for downstream effects, was innate immune response. In contrast to the early metal response, the immune response tended to hold steady or increase with exposure time over 24 h. Innate immunity is comprised of non-specific mechanisms that serve to defend a host from pathogens. Humans and *C. elegans* can be infected by many of the same pathogens [82], and while nematodes lack an adaptive immune system, conserved signaling pathways play a role in the innate immune responses of both mammals and nematodes [83]. In a recent sub-chronic study in rats using repeat intravenous dosing of AgNPs, among many toxicity endpoints assessed, it was found that immune parameters were the most responsive to AgNP exposure [84]. Immune responses were also elevated in mice in response to oral AgNP administration [80]. In *C. elegans*, we found many secreted antimicrobial CNC genes and fungal response genes were up regulated with exposure to AgNP, and that levels were higher at 24 h than at earlier time points. Exposure to 20nmAuNP did not induce any of these genes, indicating that the innate immune response to AgNP was not due to particle size, particle concentration, or NP coating. As with the metal response, exposure to Ag^+ induced nearly all of these same innate immune response genes, but without a clear pattern of timing. Taken together, our data indicate that both AgNP and Ag^+ can stimulate immune effectors, but that the effects of 12.5 μg/mL Ag^+ are far harsher and less coordinated than those of 100 μg/mL 20nmAgCit. Additionally, despite the differences between nematode and mammalian immune systems, test results from *C. elegans* correlated with those from rodents at a fraction of the time and expense, supporting the use of this model in early toxicity screens.

NP coat composition and charge can play a role in NP uptake and bioactivity. In zebrafish embryos, a PVP coat is associated with greater toxicity and increased tissue uptake relative to citrate coated AgNP of the same core size [18]. Additionally, positively charged gold nanoparticles are associated with higher mortality, and negatively charged AuNP with malformations in developing zebrafish embryos [85]. Looking at studies using various cell culture models, the effect of NP charge on cell surface absorption, uptake, and cytotoxicity is varied and sometimes contradictory [86–89]. To address this issue, we assessed the effect of coat composition on AgNP toxicity using 20 nm silver nanospheres coated with negatively charged citrate, positively charged BPEI, neutral PEG, and PVP (which carries a slight negative charge), and found that for *C. elegans* larvae, AgNP coat toxicity was ranked PEG > PVP ≅ BPEI > citrate. In toxicity assessments of these four coat compounds in the absence of silver, only BPEI was associated with toxicity at concentrations estimated to be present on the surface of 20 nm AgNP spheres at 100 μg/mL. Coating also influenced uptake, with organismal silver levels after equimolar AgNP exposure ranking PEG > PVP > citrate > BPEI. Therefore, for the coats in this study that provide neutral and negative charge, increased levels of silver uptake corresponded to increased toxicity, while positively charged BPEI did not fall in this pattern.

Our results in *C. elegans* indicating that PVP coated AgNP are associated with higher silver uptake and higher toxicity relative to similarly sized citrate coated AgNP directly corresponds to findings in a recent study using zebrafish embryos that also used 20 and 110 nm AgNP spheres [18]. In considering the implications of our finding of reduced uptake for AgNP coated with positively charged BPEI, it is important to note that the luminal pH of the *C. elegans* intestine is estimated to be in the range of 4–5 [90]. Agglomeration reduces particle bioavailability, and the aggregation state of BPEI coated AgNP, as indicated by hydrodynamic diameter, increases dramatically as pH drops below 7, and higher ionic strength results in further agglomeration at low pH [24]. Thus, in an oral exposure model, it is possible that the low toxicity of BPEI itself may have more influence than silver on BPEI-coated AgNP toxicity.

Silver nanoplates (AgPlates) are currently being studied for various biomedical applications due to the fact that they can to be "tuned" to resonate at specific frequencies by adjusting their size. As with AgNP spheres, we found that larger AgPlates were less toxic than smaller

ones, with PVP coated AgPlates that resonate at 1100 nm (average diameter of 149 nm) showing toxicity roughly equivalent to that of 110 nm PEG coated silver nanospheres, and those that resonate at 550 nm (average diameter 37 nm) being roughly equivalent to 20 nm PEG coated silver nanospheres. Thus, when comparing AgNP spheres to spheres, and plates to plates, based on mass, smaller particles were more toxic than larger ones for both shapes. If the "NP size correlates inversely with toxicity" paradigm holds when comparing the toxicity AgNPs of different shapes, this may indicate that AgNP plates are more toxic than AgNP spheres, as the larger plate (at least on the flat side) with the intermediate toxicity PVP coat was as toxic as a smaller sphere with the most toxic PEG coat.

Studies of NP safety that do not include assessments of the soluble fraction of NP suspensions run the risk of misinterpretation of effects that are the result of artifacts of manufacture or storage rather than NP exposure [16]. To separate the effects of soluble fraction components from AgNP effects, high-speed supernatants of AgNP suspensions were characterized by ICP-MS for silver content, and larval growth assays for toxicity. All of the AgNP soluble fractions contained low or non-detectable levels of silver, and none were associated with significant levels of toxicity, indicating that any toxicity detected was due to AgNP exposure.

In summary, many factors can alter the toxicity profile of nanomaterials, including size, shape, coat, charge, and methods of synthesis or purification, highlighting the need for increased levels of testing. Unlike quantitative risk assessments which provide information about specific dose levels, toxicity screening can only identify and characterize potential hazards, prioritizing compounds for further testing. Rapid predictive screening methods are required to keep up with increases in the development of products containing AgNP, and will allow more efficient use of expensive and lengthy traditional toxicity assessments. Data presented here using *C. elegans* correlates well with findings in rodents for AgNP size vs. uptake and toxicity, as well as for induction of immune effectors, while other findings such as PVP coats imparting higher toxicity to AgNP that citrate are ahead of testing in mammals, but correlate with data in zebrafish, supporting the use of *C. elegans* as an alternative model for toxicity screening.

5. Conclusions

As in rodents, nanosilver is less toxic than ionic silver to *C. elegans*, and decreasing size correlates with increasing toxicity and increasing organismal silver uptake, indicating the potential of this model to predict mammalian response. Of the four nanomaterial coatings assessed in this study, citrate was the least toxic, PEG was the most toxic, and PVP and BPEI imparted intermediate levels of toxicity to 20 nm silver spheres. For nanosilver spheres with neutral or negative zeta potentials, higher levels of silver uptake correlated with increased toxicity. This pattern did not hold for positively charged silver nanospheres or for nanoplates, indicating that increased nanosilver toxicity does not necessarily correspond with increased silver uptake. Gene regulation in response to nanosilver exposure indicated early metal and stress responses, and sustained or late immune responses. Most of the metal, stress, and immune response genes differentially regulated by nanosilver were also regulated by ionic silver exposure, in many cases to far greater extents and without the early/late timing patterns.

Declarations

This manuscript reflects the views of the authors and should not be construed to represent views or policies of the U.S. Food and Drug Administration (FDA). S.J.O. is employed by nanoComposix, which under a material transfer agreement with the FDA Center for Food Safety and Applied Nutrition, fabricated and characterized all nanomaterials used in this study. The remaining authors declare they have no financial or personal association with any individuals or organizations that could inappropriately influence the submitted work.

Conflict of interest

None declared.

Transparency document

The Transparency document associated with this article can be found in the online version.

Appendix A. Supplementary data

Supplementary data associated with this article can be found, in the online version, at doi:10.1016/j.toxrep.2014.10.020.

References

[1] J.D. Watson, F.H. Crick, Molecular structure of nucleic acids: a structure for deoxyribose nucleic acid, Nature 171 (4356) (1953) 737–738.
[2] J.P. Abrahams, A.G. Leslie, et al., Structure at 2.8 A resolution of F1-ATPase from bovine heart mitochondria, Nature 370 (6491) (1994) 621–628.
[3] J. Dittman, T.A. Ryan, Molecular circuitry of endocytosis at nerve terminals, Annu. Rev. Cell Dev. Biol. 25 (2009) 133–160.
[4] S.E. McNeil, Nanotechnology for the biologist, J. Leukoc. Biol. 78 (3) (2005) 585–594.
[5] C.-F. Chau, S.-H. Wu, et al., The development of regulations for food nanotechnology, Trends Food Sci. Technol. 18 (5) (2007) 269–280.
[6] Project-on-Emerging-Technologies, Nanotechnology-based consumer products analysis, in: Consumer Products, 2013, March 10, 2011, http://www.nanotechproject.org/inventories/consumer/analysis_draft/ (retrieved 22.10.13).
[7] T. Xia, N. Li, et al., Potential health impact of nanoparticles, Annu. Rev. Public Health 30 (2009) 137–150.
[8] I. Sondi, B. Salopek-Sondi, Silver nanoparticles as antimicrobial agent: a case study on *E. coli* as a model for Gram-negative bacteria, J. Colloid Interface Sci. 275 (1) (2004) 177–182.
[9] J.L. Elechiguerra, J.L. Burt, et al., Interaction of silver nanoparticles with HIV-1, J. Nanobiotechnol. 3 (2005) 6.
[10] H.H. Lara, N.V. Ayala-Nunez, et al., Mode of antiviral action of silver nanoparticles against HIV-1, J. Nanobiotechnol. 8 (2010) 1.
[11] F. Martinez-Gutierrez, P.L. Olive, et al., Synthesis, characterization, and evaluation of antimicrobial and cytotoxic effect of silver and titanium nanoparticles, Nanomedicine 6 (5) (2010) 681–688.
[12] F. Martinez-Gutierrez, E.P. Thi, et al., Antibacterial activity, inflammatory response, coagulation and cytotoxicity effects of silver nanoparticles, Nanomedicine 8 (3) (2012) 328–336.

[13] B. Nowack, H.F. Krug, et al., 120 years of nanosilver history: implications for policy makers, Environ. Sci. Technol. 45 (4) (2011) 1177–1183.
[14] J.W. Card, T.S. Jonaitis, et al., An appraisal of the published literature on the safety and toxicity of food-related nanomaterials, Crit. Rev. Toxicol. 41 (1) (2011) 22–49.
[15] S. Kittler, C. Greulich, et al., Toxicity of silver nanoparticles increases during storage because of slow dissolution under release of silver ions, Chem. Mater. 22 (16) (2010) 4548–4554.
[16] M. van der Zande, R.J. Vandebriel, et al., Distribution, elimination, and toxicity of silver nanoparticles and silver ions in rats after 28-day oral exposure, ACS Nano 6 (8) (2012) 7427–7442.
[17] J.R. Morones, J.L. Elechiguerra, et al., The bactericidal effect of silver nanoparticles, Nanotechnology 16 (10) (2005) 2346–2353.
[18] K.-T. Kim, L. Truong, et al., Silver nanoparticle toxicity in the embryonic zebrafish is governed by particle dispersion and ionic environment, Nanotechnology 24 (2013) 1–8.
[19] M.V. Park, A.M. Neigh, et al., The effect of particle size on the cytotoxicity, inflammation, developmental toxicity and genotoxicity of silver nanoparticles, Biomaterials 32 (36) (2011) 9810–9817.
[20] K.A. Homan, M. Souza, et al., Silver nanoplate contrast agents for in vivo molecular photoacoustic imaging, ACS Nano 6 (1) (2012) 641–650.
[21] S. Pal, Y.K. Tak, et al., Does the antibacterial activity of silver nanoparticles depend on the shape of the nanoparticle? A study of the Gram-negative bacterium *Escherichia coli*, Appl. Environ. Microbiol. 73 (6) (2007) 1712–1720.
[22] S. George, S. Lin, et al., Surface defects on plate-shaped silver nanoparticles contribute to its hazard potential in a fish gill cell line and zebrafish embryos, ACS Nano 6 (5) (2012) 3745–3759.
[23] T.M. Tolaymat, A.M. El Badawy, et al., An evidence-based environmental perspective of manufactured silver nanoparticle in syntheses and applications: a systematic review and critical appraisal of peer-reviewed scientific papers, Sci. Total Environ. 408 (5) (2010) 999–1006.
[24] A.M. El Badawy, T.P. Luxton, et al., Impact of environmental conditions (pH, ionic strength, and electrolyte type) on the surface charge and aggregation of silver nanoparticles suspensions, Environ. Sci. Technol. 44 (4) (2010) 1260–1266.
[25] S. Tan, M. Erol, et al., Synthesis of positively charged silver nanoparticles via photoreduction of $AgNO_3$ in branched polyethyleneimine/HEPES solutions, Langmuir 23 (19) (2007) 9836–9843.
[26] P. Thevenot, J. Cho, et al., Surface chemistry influences cancer killing effect of TiO_2 nanoparticles, Nanomedicine 4 (3) (2008) 226–236.
[27] W. Eck, G. Craig, et al., PEGylated gold nanoparticles conjugated to monoclonal F19 antibodies as targeted labeling agents for human pancreatic carcinoma tissue, ACS Nano 2 (11) (2008) 2263–2272.
[28] M.A. Dobrovolskaia, S.E. McNeil, Immunological properties of engineered nanomaterials, Nat. Nanotechnol. 2 (8) (2007) 469–478.
[29] J. Costanza, A.M. El Badawy, et al., Comment on 120 Years of nanosilver history: implications for policy makers, Environ. Sci. Technol. 45 (17) (2011) 7591–7592, author reply 7593–7595.
[30] P.R. Hunt, B.J. Marquis, et al., Nanosilver suppresses growth and induces oxidative damage to DNA in *Caenorhabditis elegans*, J. Appl. Toxicol. 33 (10) (2013) 1131–1142.
[31] G. Oberdorster, Safety assessment for nanotechnology and nanomedicine: concepts of nanotoxicology, J. Intern. Med. 267 (1) (2010) 89–105.
[32] C.M. Sayes, K.L. Reed, et al., Assessing toxicity of fine and nanoparticles: comparing in vitro measurements to in vivo pulmonary toxicity profiles, Toxicol. Sci. 97 (1) (2007) 163–180.
[33] K.S. Betts, Tox21 to date: steps toward modernizing human hazard characterization, Environ. Health Perspect. 121 (7) (2013) a228.
[34] R.L. Sprando, N. Olejnik, et al., A method to rank order water soluble compounds according to their toxicity using *Caenorhabditis elegans*, a complex object parametric analyzer and sorter, and axenic liquid media, Food Chem. Toxicol. 47 (4) (2009) 722–728.
[35] W.A. Boyd, S.J. McBride, et al., A high-throughput method for assessing chemical toxicity using a *Caenorhabditis elegans* reproduction assay, Toxicol. Appl. Pharmacol. 245 (2) (2010) 153–159.
[36] P.R. Hunt, N. Olejnik, et al., Toxicity ranking of heavy metals with screening method using adult *Caenorhabditis elegans* and propidium iodide replicates toxicity ranking in rat, Food Chem. Toxicol. 50 (9) (2012) 3280–3290.
[37] nanoComposix, Guidelines for Nanotoxicology Researchers Using nanoComposix Materials. v1.1, 2012, September, http://cdn.shopify.com/s/files/1/0257/8237/files/nanoComposix_Guidelines_for_Nanotox_Researchers.pdf?13692 (retrieved 09.07.14).
[38] W. Tong, X. Cao, et al., ArrayTrack – supporting toxicogenomic research at the U.S. Food and Drug Administration National Center for Toxicological Research, Environ. Health Perspect. 111 (15) (2003) 1819–1826.
[39] R.A. Irizarry, B. Hobbs, et al., Exploration, normalization, and summaries of high density oligonucleotide array probe level data, Biostatistics 4 (2) (2003) 249–264.
[40] S. Hochreiter, D.A. Clevert, et al., A new summarization method for Affymetrix probe level data, Bioinformatics 22 (8) (2006) 943–949.
[41] K.L. Kelly, E. Coronado, et al., The optical properties of metal nanoparticles: the influence of size, shape, and dielectric environment, J. Phys. Chem. B 107 (3) (2003) 668–677.
[42] N. Hadrup, K. Loeschner, et al., Subacute oral toxicity investigation of nanoparticulate and ionic silver in rats, Arch. Toxicol. 86 (4) (2012) 543–551.
[43] N. Pujol, O. Zugasti, et al., Anti-fungal innate immunity in *C. elegans* is enhanced by evolutionary diversification of antimicrobial peptides, PLoS Pathog. 4 (7) (2008) e1000105.
[44] WormBase (2014). www.wormbase.org (retrieved 30.05.14).
[45] R.S. Friling, A. Bensimon, et al., Xenobiotic-inducible expression of murine glutathione S-transferase Ya subunit gene is controlled by an electrophile-responsive element, Proc. Natl. Acad. Sci. U. S. A. 87 (16) (1990) 6258–6262.
[46] M.B. Fisher, M.F. Paine, et al., The role of hepatic and extrahepatic UDP-glucuronosyltransferases in human drug metabolism, Drug Metab. Rev. 33 (3–4) (2001) 273–297.
[47] W. Huang da, B.T. Sherman, et al., Bioinformatics enrichment tools: paths toward the comprehensive functional analysis of large gene lists, Nucleic Acids Res. 37 (1) (2009) 1–13.
[48] W. Huang da, B.T. Sherman, et al., Systematic and integrative analysis of large gene lists using DAVID bioinformatics resources, Nat. Protoc. 4 (1) (2009) 44–57.
[49] OMIM, Online Mendelian Inheritance in Man, 2014, http://omim.org (retrieved 30.05.14).
[50] Google Scholar, 2014, http:scholar.google.com (retrieved 30.05.14).
[51] D. O'Rourke, D. Baban, et al., Genomic clusters, putative pathogen recognition molecules, and antimicrobial genes are induced by infection of *C. elegans* with *M. nematophilum*, Genome Res. 16 (8) (2006) 1005–1016.
[52] M. Shapira, B.J. Hamlin, et al., A conserved role for a GATA transcription factor in regulating epithelial innate immune responses, Proc. Natl. Acad. Sci. U. S. A. 103 (38) (2006) 14086–14091.
[53] E.R. Troemel, S.W. Chu, et al., p38 MAPK regulates expression of immune response genes and contributes to longevity in *C. elegans*, PLoS Genet. 2 (11) (2006) e183.
[54] R.E. Muir, M.W. Tan, Virulence of *Leucobacter chromiireducens* subsp. *solipictus* to *Caenorhabditis elegans*: characterization of a novel host–pathogen interaction, Appl. Environ. Microbiol. 74 (13) (2008) 4185–4198.
[55] R. Pukkila-Worley, F.M. Ausubel, et al., Candida albicans infection of *Caenorhabditis elegans* induces antifungal immune defenses, PLoS Pathog. 7 (6) (2011) e1002074.
[56] S.N. Sahu, J. Lewis, et al., Genomic analysis of immune response against *Vibrio cholerae* hemolysin in *Caenorhabditis elegans*, PLoS ONE 7 (5) (2012) e38200.
[57] D. Wong, D. Bazopoulou, et al., Genome-wide investigation reveals pathogen-specific and shared signatures in the response of *Caenorhabditis elegans* to infection, Genome Biol. 8 (9) (2007) R194.
[58] M.K. McElwee, L.A. Ho, et al., Comparative toxicogenomic responses of mercuric and methyl-mercury, BMC Genomics 14 (2013) 698.
[59] J.-Y. Roh, S.-Y. Park, et al., Cadmium toxicity monitoring using stress related gene expressions in *Caenorhabditis elegans*, Mol. Cell. Toxicol. 2 (1) (2006) 54–59.
[60] Y. Cui, S.J. McBride, et al., Toxicogenomic analysis of *Caenorhabditis elegans* reveals novel genes and pathways involved in the resistance to cadmium toxicity, Genome Biol. 8 (6) (2007) R122.
[61] S.N. Sahu, J. Lewis, et al., Genomic analysis of stress response against arsenic in *Caenorhabditis elegans*, PLOS ONE 8 (7) (2013) e66431.
[62] J.A. Lewis, E.A. Gehman, et al., Alterations in gene expression in *Caenorhabditis elegans* associated with organophosphate pesticide intoxication and recovery, BMC Genomics 14 (2013) 291.
[63] A.J. Przybysz, K.P. Choe, et al., Increased age reduces DAF-16 and SKN-1 signaling and the hormetic response of *Caenorhabditis elegans* to the xenobiotic juglone, Mech. Ageing Dev. 130 (6) (2009) 357–369.
[64] H. Shin, H. Lee, et al., Gene expression profiling of oxidative stress response of *C. elegans* aging defective AMPK mutants using massively parallel transcriptome sequencing, BMC Res. Notes 4 (2011) 34.

[65] A.S. Dawe, R.K. Bodhicharla, et al., Low-intensity microwave irradiation does not substantially alter gene expression in late larval and adult *Caenorhabditis elegans*, Bioelectromagnetics 30 (8) (2009) 602–612.
[66] J.Y. Kwon, M. Hong, et al., Ethanol-response genes and their regulation analyzed by a microarray and comparative genomic approach in the nematode *Caenorhabditis elegans*, Genomics 83 (4) (2004) 600–614.
[67] J.Y. Roh, I.H. Jung, et al., Toxic effects of di(2-ethylhexyl)phthalate on mortality, growth, reproduction and stress-related gene expression in the soil nematode *Caenorhabditis elegans*, Toxicology 237 (1–3) (2007) 126–133.
[68] J.A. Lewis, M. Szilagyi, et al., Distinct patterns of gene and protein expression elicited by organophosphorus pesticides in *Caenorhabditis elegans*, BMC Genomics 10 (2009) 202.
[69] A. Vinuela, L.B. Snoek, et al., Genome-wide gene expression analysis in response to organophosphorus pesticide chlorpyrifos and diazinon in *C. elegans*, PLoS ONE 5 (8) (2010) e12145.
[70] K. Reichert, R. Menzel, Expression profiling of five different xenobiotics using a *Caenorhabditis elegans* whole genome microarray, Chemosphere 61 (2) (2005) 229–237.
[71] K. Hasegawa, S. Miwa, et al., Acrylamide-responsive genes in the nematode *Caenorhabditis elegans*, Toxicol. Sci. 101 (2) (2008) 215–225.
[72] S.J. Lee, C.T. Murphy, et al., Glucose shortens the life span of *C. elegans* by downregulating DAF-16/FOXO activity and aquaporin gene expression, Cell Metab. 10 (5) (2009) 379–391.
[73] C.E. Schwerdt, F.L. Schaffer, Some physical and chemical properties of purified poliomyelitis virus preparations, Ann. N. Y. Acad. Sci. 61 (4) (1955) 740–750, discussion 750–743.
[74] D.C. Stuart Jr., Virology 13 (2) (1961) 177–190.
[75] C. Wallis, J.L. Melnick, Virus aggregation as the cause of the non-neutralizable persistent fraction, J. Virol. 1 (3) (1967) 478–488.
[76] T. Fifis, A. Gamvrellis, et al., Size-dependent immunogenicity: therapeutic and protective properties of nano-vaccines against tumors, J. Immunol. 173 (5) (2004) 3148–3154.
[77] Y. Matuk, M. Ghosh, et al., Distribution of silver in the eyes and plasma proteins of the albino rat, Can. J. Ophthalmol. 16 (3) (1981) 145–150.
[78] Y.S. Kim, M.Y. Song, et al., Subchronic oral toxicity of silver nanoparticles, Part. Fibre Toxicol. 7 (2010) 20.
[79] K. Loeschner, N. Hadrup, et al., Distribution of silver in rats following 28 days of repeated oral exposure to silver nanoparticles or silver acetate, Part. Fibre Toxicol. 8 (2011) 18.
[80] E.J. Park, E. Bae, et al., Repeated-dose toxicity and inflammatory responses in mice by oral administration of silver nanoparticles, Environ. Toxicol. Pharmacol. 30 (2) (2010) 162–168.
[81] J.Y. Roh, S.J. Sim, et al., Ecotoxicity of silver nanoparticles on the soil nematode *Caenorhabditis elegans* using functional ecotoxicogenomics, Environ. Sci. Technol. 43 (10) (2009) 3933–3940.
[82] C.D. Sifri, J. Begun, et al., The worm has turned – microbial virulence modeled in *Caenorhabditis elegans*, Trends Microbiol. 13 (3) (2005) 119–127.
[83] J.E. Irazoqui, A. Ng, et al., Role for beta-catenin and HOX transcription factors in *Caenorhabditis elegans* and mammalian host epithelial–pathogen interactions, Proc. Natl. Acad. Sci. U. S. A. 105 (45) (2008) 17469–17474.
[84] W.H. De Jong, L.T. Van Der Ven, et al., Systemic and immunotoxicity of silver nanoparticles in an intravenous 28 days repeated dose toxicity study in rats, Biomaterials 34 (33) (2013) 8333–8343.
[85] S.L. Harper, J.L. Carriere, et al., Systematic evaluation of nanomaterial toxicity: utility of standardized materials and rapid assays, ACS Nano 5 (6) (2011) 4688–4697.
[86] C.M. Goodman, C.D. McCusker, et al., Toxicity of gold nanoparticles functionalized with cationic and anionic side chains, Bioconjug. Chem. 15 (4) (2004) 897–900.
[87] C. He, Y. Hu, et al., Effects of particle size and surface charge on cellular uptake and biodistribution of polymeric nanoparticles, Biomaterials 31 (13) (2010) 3657–3666.
[88] A. Verma, F. Stellacci, Effect of surface properties on nanoparticle–cell interactions, Small 6 (1) (2010) 12–21.
[89] O. Lee, S.H. Jeong, et al., Influence of surface charge of gold nanorods on skin penetration, Skin Res. Technol. 19 (1) (2013) e390–e396.
[90] J.D. McGhee, The *C. elegans* intestine, in: WormBook, The *C. elegans* Research Community, 2007, http://dx.doi.org/10.1895/wormbook.1.133.1.